Since January 2020 Elsevier has created a COVID-19 resource centre with free information in English and Mandarin on the novel coronavirus COVID-19. The COVID-19 resource centre is hosted on Elsevier Connect, the company's public news and information website.

Expert Systems With Applications 213 (2023) 119095

Contents lists available at ScienceDirect

Expert Systems With Applications

journal homepage: www.elsevier.com/locate/eswa

Boosted crow search algorithm for handling multi-threshold image problems with application to X-ray images of COVID-19

Songwei Zhao [a], Pengjun Wang [b,*], Ali Asghar Heidari [a,c,1], Xuehua Zhao [d], Huiling Chen [a,*]

[a] College of Computer Science and Artificial Intelligence, Wenzhou University, Wenzhou, Zhejiang 325035, China
[b] College of Electrical and Electronic Engineering, Wenzhou University, Wenzhou 325035, China
[c] School of Surveying and Geospatial Engineering, College of Engineering, University of Tehran, Tehran, Iran
[d] School of Digital Media, Shenzhen Institute of Information Technology, Shenzhen 518172, China

ARTICLE INFO

Keywords:
Multi-threshold image segmentation
Crow search algorithm
Renyi's entropy
2D histogram
COVID-19
Optimization

ABSTRACT

COVID-19 is pervasive and threatens the safety of people around the world. Therefore, now, a method is needed to diagnose COVID-19 accurately. The identification of COVID-19 by X-ray images is a common method. The target area is extracted from the X-ray images by image segmentation to improve classification efficiency and help doctors make a diagnosis. In this paper, we propose an improved crow search algorithm (CSA) based on variable neighborhood descent (VND) and information exchange mutation (IEM) strategies, called VMCSA. The original CSA quickly falls into the local optimum, and the possibility of finding the best solution is significantly reduced. Therefore, to help the algorithm avoid falling into local optimality and improve the global search capability of the algorithm, we introduce VND and IEM into CSA. Comparative experiments are conducted at CEC2014 and CEC'21 to demonstrate the better performance of the proposed algorithm in optimization. We also apply the proposed algorithm to multi-level thresholding image segmentation using Renyi's entropy as the objective function to find the optimal threshold, where we construct 2-D histograms with grayscale images and non-local mean images and maximize the Renyi's entropy on top of the 2-D histogram. The proposed segmentation method is evaluated on X-ray images of COVID-19 and compared with some algorithms. VMCSA has a significant advantage in segmentation results and obtains better robustness than other algorithms. The available extra info can be found at https://github.com/1234zsw/VMCSA.

1. Introduction

In late 2019, a new coronavirus disease, called COVID-19, first broke out suddenly in Wuhan, China, followed by a subsequent emergence of COVID-19 worldwide (Di Buo et al., 2021; Mukhtar & Rana, 2021). Initially, there was insufficient understanding of COVID-19 and no precise diagnostic methods, leading to the rapid spread of the virus in the population and a severe threat to people's lives. Patients with COVID-19 have an incubation period at first, followed by symptoms such as fever, fatigue, and sore throat, and can also lead to pneumonia. COVID-19 severely impacts people's safety worldwide and the economic development of countries (Aneja et al., 2021; Jalušić Glunčić et al., 2021), so a tool is needed to detect the virus early and provide timely treatment. To date, chest X-rays images play a crucial part in the diagnosis of COVID-19; the resultant X-ray images are extracted as normal images and are segmented into small regions with different information, some of which may contain features of COVID-19, and this process is commonly referred to as the image segmentation (IS) problem (Amyar, Modzelewski, Li, & Ruan, 2020; Chen, Yao, Zhou, Dong, & Zhang, 2021; Di et al., 2021).

IS is a crucial image processing stage and has been widely used in many fields (Houssein, Helmy, Oliva, Elngar, & Shaban, 2021; Merzban & Elbayoumi, 2019). It is the process of segmenting different regions of an image with special meanings based on the image's grayscale, texture, and color, where each region does not intersect with each other, and each region satisfies the consistency of a particular region. A variety of segmentation methods (e.g., region-based (Zhang et al., 2016), artificial intelligence-based (Xia, Liu, & Huang, 2021), edge detection-based (Michetti, Georgelin-Gurgel, Mallet, Diemer, & Boulanouar, 2015), and active contour model-based segmentation methods (Dong, Jin, &

* Corresponding authors.
E-mail addresses: wangpengjun@wzu.edu.cn (P. Wang), as_heidari@ut.ac.ir (A.A. Heidari), zhaoxh@sziit.edu.cn (X. Zhao), chenhuiling.jlu@gmail.com (H. Chen).
[1] https://aliasgharheidari.com

https://doi.org/10.1016/j.eswa.2022.119095
Received 28 July 2021; Received in revised form 11 October 2022; Accepted 18 October 2022
Available online 22 October 2022

Weng, 2019)) have been used to solve the currently existing problem. Threshold IS is the most common and fundamental of IS techniques. Based on the number of thresholds, it is classified into two kinds: two-level and multi-level thresholding. Multi-level thresholding image segmentation (MTIS) has better results in dealing with complex images. There are two methods to find the threshold values: non-parametric and parametric. The non-parametric method maximizes some functions including Renyi's entropy (Nobre et al., 2016; Zhao et al., 2021), Kapur's entropy (Abdel-Basset, Chang, & Mohamed, 2020; Aranguren, Valdivia, Morales-Castañeda et al., 2021; Zhao, Liu, Yu, Heidari, Wang, Liang et al., 2020; Zhao, Liu, Yu, Heidari, Wang, Oliva et al., 2020) and fuzzy entropy (Yin, Qian, & Gong, 2017; Yu, Zhi, & Fan, 2015). The parametric method requires using probability density functions to identify each class of images. Nowadays, many algorithms have been used to overcome the nonparametric MTIS problem. However, these algorithms still have some problems obtaining accurate segmented images, and the increase of threshold value brings a greater time complexity, and the traditional methods cannot meet the current demand. Therefore, the urgent need for a robust algorithm to solve the MTIS problem has increased significantly, especially for X-ray images of COVID-19.

Optimization problems can be divided according to different measures based on the accuracy of the mathematical foundation or application area (Zhang, Chen, & Lin, 2021; Zhang, Chen, & Susilo, 2020), but generally, there are single objective problems and multi-objective cases (Cao et al., 2022; Lu, Liu, Zhang, & Yin, 2022). In recent years, metaheuristic algorithms (Mas) have been used as tools by researchers to solve problems. Since MAs are easy to understand and realize, they have been noticed and used by researchers to solve multi-threshold finding problems in MTIS. Some of the MAs that have received attention include the Salp Swarm Algorithm (SSA) (Mirjalili, Dong, & Lewis, 2019) based on Salps foraging, Gray Wolf Optimization (GWO) (Mirjalili et al., 2019) based on gray wolves hunting, Equilibrium Optimizer (IEO) (Zhu et al., 2022), Whale Optimization Algorithm (WOA) (Mirjalili et al., 2019) based on whales spiral hunting, Differential Evolution (DE) (Mirjalili et al., 2019) based on genetic crossover and mutations, Runge Kutta Optimizer (RUN) (Ahmadianfar, Heidari, Gandomi, Chu, & Chen, 2021) based on math, Colony Predation Algorithm (CPA) (Tu, Chen, Wang, & Gandomi, 2021) based on logic of animals, Weighted Mean of Vectors (INFO) (Ahmadianfar, Heidari, Noshadian, Chen, & Gandomi, 2022) based on math rules, Hunger Games Search (HGS) (Yang, Chen, Heidari, & Gandomi, 2021) based on hunger feel of animals, Harris Hawk Optimizer (HHO) (Heidari, Mirjalili et al., 2019) based on Harris hawks foraging, Bat Algorithm (BA) (Mirjalili et al., 2019) based on acoustic echolocation, Particle Swarm Optimization (PSO) (Cao et al., 2021) based on bird population behavior, and Slime Mould Algorithm (SMA) (Li, Chen, Wang, Heidari, & Mirjalili, 2020) based on slimes foraging. Furthermore, they also have been applied many various fields, such as economic emission dispatch problem (Dong et al., 2021), image segmentation (Hussien et al., 2022; Yu, Song et al., 2022), feature selection (Hu et al., 2021; Hu et al., 2022), medical diagnosis (Cai et al., 2018; Li et al., 2017), expensive optimization problems (Li, Zhan, Wang, Jin, & Zhang, 2020; Wu, Zhan, & Zhang, 2021), fault diagnosis (Yu et al., 2021), solar cell parameter identification (Ye et al., 2021), plant disease recognition (Yu, Cheng et al., 2022), bankruptcy prediction (Cai et al., 2019; Xu et al., 2019), combination optimization problems (Zhao, Di, Cao, & Tang, 2021), optimization of machine learning model (ling Chen et al., 2014), robust optimization (He, Yen, & Ding, 2020; He, Yen, & Lv, 2019; He, Yen, & Yi, 2018), multi-objective problem (Deng et al., 2022; Hua, Liu, Hao, & Jin, 2021), and global optimization (Chen et al., 2020; Wang et al., 2021). Among them, Askarzadeh (Askarzadeh, 2016) proposed Crow Search Algorithm (CSA) based on crows hiding and retrieving food, which showed better results in some constrained engineering problems. Therefore, in this work, CSA is chosen as a new method for solving the chest X-ray MTIS problem, which is used to separate the region of interest inside the X-ray image.

Researchers have received CSA well in recent years, and much work has been done to improve it. Al-Thanoon, Algamal, and Qasim (2021) proposed to improve the binary CSA, named OBLBCSA, based on an opposition-based learning strategy to determine the flight parameters. The experimental results showed that the method outperformed other arithmetic methods regarding relevant feature selection for both data sets. Chaudhuri and Sahu (2021) proposed the Binary CSA with Time-Varying Flight Length (BCSA-TVFL) for the drawback that the original CSA is prone to fall into local optimality when solving the feature selection problem in packing mode. CSA was improved (I-CSA) through discretization, local search, and elitism by Eliguzel and Ozceylan (2021) and successfully applied to the P-median problem. Gholami, Mardukhi, and Zawbaa (2021) improved CSA (ICSA) by using the update mechanism that moves the advantage of the global best position to the best position, which better helps the algorithm to avoid premature convergence and improves the local search ability and convergence speed of the algorithm. Ke, Xie, and Pouramini (2021) improved CSA through reverse learning and value functions with good results in the optimal design of a typical commercial building in a selected Australian city. Necira, Naimi, Salhi, Salhi, and Menani (2021) proposed a dynamic CSA (DCSA) based on linearly adjusted perceptual probability and flight length adjusted by generalized Pareto probability density function to address the ease of falling into local optimum defect caused by fixed flight length and perceptual probability in CSA.

Cao, Yue, Zhang, and Cai (2021) improved the global search capability and convergence accuracy of the original algorithm by incorporating the search strategy of the particle swarm algorithm and Gaussian function into the CSA. This variant was used to optimize the extreme learning machine. Farh, Eltamaly, Al-Shaalan, and Al-Shamma'a (2021) selected the optimal buses by hybrid CSA and particle swarm optimization algorithm in the distributed generation scale allocation problem, effectively reducing the power loss and total cost and relieving the line load. Ouadfel and Abd Elaziz (2020) proposed an enhanced CSA (ECSA) with three strategies of adaptive perceptual probability, dynamic local domain search, and novel global search, and used this method as a feature selection method for wrappers to extract the best subset of features. Khalilpourazari and Pasandideh (2020) remarkably improved the exploration and development of algorithms by mixing the sine - cosine algorithm and CSA. Diaz et al. (2018) enhanced the algorithm's convergence to complicated high multimodal optimal solutions by improving the perceptual probability and random perturbation of the original CSA, and obtained better results in solving complex energy optimization problems. Rizk-Allah, Hassanien, and Bhattacharyya (2018) proposed to combine chaos theory with CSA (CCSA) to boost the exploration/exploitation capability and global search capability of the algorithm, and used the method to solve fractional optimization problems. Jain, Rani, and Singh (2017) introduced adaptive adjustment operator, Levy flight distribution, and experience factor in CSA, which effectively balanced the exploration and exploitation of variants and achieved better results in solving high-dimensional global optimization problems.

Although these improved CSAs have achieved better results in different areas, they are still limited in finding the optimal solution. According to the No-Free-Lunch (NFL) (Wolpert & Macready, 1997), no single algorithm can outperform all other algorithms on all problems. Therefore, it is necessary to improve some simple algorithms or propose new algorithms to solve certain cases better. This motivates us to propose an improved CSA, VMCSA, to improve its performance on MTIS. The improved variants exhibit higher accuracy and convergence speed in handling the MTIS problems and benchmark test set based on these two strategies.

The contributions and innovations of this paper are as follows:

- To increase the probability of finding the optimal solution for CSA, we introduced two strategies, VND and IEM, to propose VMCSA improvement variants, the former increasing the diversity of

Table 1
Some algorithms proposed for solving the MTIS problem.

Reference	Method
Abd Elaziz *et al.* (Abd Elaziz et al., 2021)	This paper proposed a multi-leader whale optimization algorithm (MLWOA) to come out of the IS problem, which can effectively avoid falling into the local optimum in the search process.
Kalyani *et al.* (Kalyani, Sathya, & Sakthivel, 2021)	This paper proposed the exchange market algorithm (EMA) to solve the MTIS problem based on Tsallis and Renyi, reducing the computation time to explore the optimal threshold.
Renugambal *et al.* (Renugambal & Selva Bhuvaneswari, 2021)	This paper hybridizes the water cycle and moth-flame optimization (WCMFO) algorithm to improve the exploration and exploitation capabilities and find the optimal threshold for complex brain images by maximizing Kapur's entropy.
Houssein *et al.* (Houssein et al., 2021)	This paper introduces a new MA, black widow optimization (BWO), to find the optimal threshold combination by using Otsu or Kapur as the objective function.
Aranguren et al. (Aranguren, Valdivia, Morales-Castaneda et al., 2021)	This paper used a robust MA called adaptive differential evolution (LSHADE), which can adjust the internal parameters based on the prior knowledge obtained during the evolution process.
Rahaman *et al.* (Rahaman & Sing, 2021)	This paper proposes a novel adaptive cuckoo search (ACS) algorithm to solve the IS problem by optimizing both Otsu's method and Tsallis entropy objective functions.
Yan *et al.* (Yan et al., 2020)	This paper segments underwater images using a modified water wave optimization (MWWO) algorithm. MWWO can effectively balance exploration and exploitation and increase the possibility of finding the optimal solution.
Upadhyay *et al.* (Upadhyay & Chhabra, 2020)	This paper proposed CSA to evaluate the optimal threshold combination problem in MTIS by maximizing Kapur's entropy. The method achieves better experimental results due to the advantages such as fewer parameters.
Khairuzzaman *et al.* (Khairuzzaman & Chaudhury, 2020)	This paper has improved the moth-flame optimization (MFO) algorithm and applied it to the MTIS problem by using cross-entropy as the objective function to choose the best threshold.
Luo *et al.* (Luo et al., 2019)	In this paper, an improved adaptive differential evolution (JADE) algorithm was proposed and used to solve the optimal threshold for MTIS of 2D Otsu with significant improvements in terms of segmentation speed and accuracy.
Zhou *et al.* (Zhou et al., 2018)	In this paper, to overcome the drawback that the computational complexity increases exponentially with the increase of thresholds, an MTIS method based on the moth swarm algorithm has been proposed.
Singla *et al.* (Singla & Patra, 2017)	This paper used clustering validity measures to determine the number and bounds of optimal thresholds, then a genetic algorithm (GA) was used to detect the optimal values from the bounds of the thresholds.

algorithms and improving the exploration capability. In comparison, the latter strategy increases the exploitation capability of the algorithm and improves the convergence performance.

- The proposed VMCSA exhibits outstanding optimization performance and convergence speed compared to main methods clearly suitable for different benchmark test conditions, including CEC2014 (Chen, Zheng, Liu, & Xie, 2014) and CEC21 (Bujok & Kolenovsky, 2021) function sets.
- We also applied VMCSA to the MTIS problem for COVID-19 X-ray images to assist in accurately finding the optimal threshold or approximating the optimal threshold, helping physicians make the correct diagnosis one at a time. The experimental results show that the proposed algorithm has high competitiveness and robustness.

The rest of the paper is arranged below: An explanation of some literature related to MTIS is in Section 2. The methods being used in the article are described in Section 3. The introduction of the proposed method is presented in Section 4. The experimental results of the proposed method are analyzed and discussed in Section 5. In the end, the summary of the whole article and an outlook on future research are presented.

2. Literature review about MTIS

IS is a key technology in image processing to analyze aspects in the fields of image recognition, medical imaging and unmanned aircraft, and so on. Although there are a number of methods to tackle IS, MTIS is now the most widely used technique and is trusted by researchers. However, the increase in threshold level leads to larger time complexity, so the traditional threshold finding technique cannot meet the current demand. Moreover, in solving constrained problems like these, MAs can effectively avoid such problems. This section presents an outline of the recent work on MAs in IS.

Abd Elaziz, Lu, and He (2021) proposed an MTIS method based on improving the performance of WOA. The experimental results show that the proposed method has a high advantage in the performance index of IS. Kalyani, Sathya, & Sakthivel, 2021 proposed an MTIS method based on the Exchange Market Algorithm and proved experimentally that the method outperforms other algorithms. Renugambal and Selva Bhuvaneswari (2021) proposed to combine the Water Cycle Algorithm with the Moth Flame Algorithm (WCMFO) to solve brain MR IS. Experiments revealed the performance preference of multi-level threshold-based WCMFO for segmenting complex brain images. Houssein, Helmy, Oliva, Elngar, and Shaban (2021) proposed a novel metaheuristic algorithm named Black Widow Optimization and used Otsu or Kapur as the objective function to search for the optimal threshold. Aranguren et al. (2021) proposed an LSHADE-based MTIS method and used it to segment MRI. Statistical validation showed that the method effectively improved the segmentation quality. Rahaman and Sing (2021) proposed a novel adaptive Cuckoo Algorithm to effectively solve the satellite IS problem. The excellence of the method was demonstrated by evaluating several metrics. Yan, Zhang, and Tang (2020) used an improved Water Wave

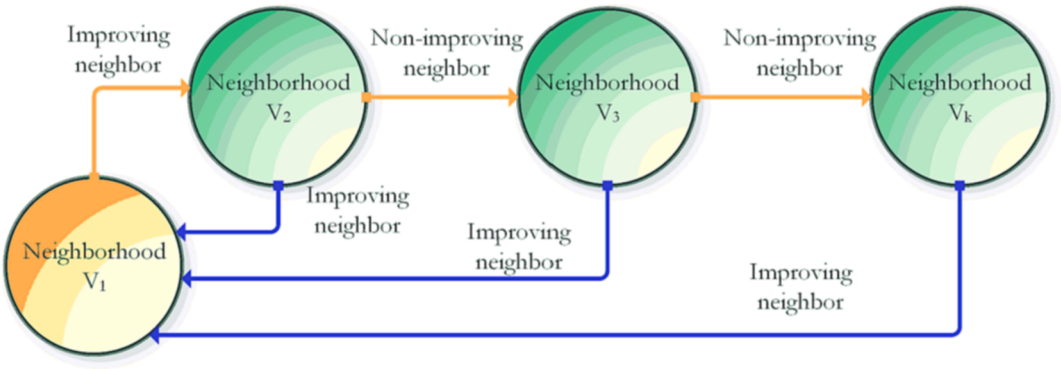

Fig. 1. Illustration of VND.

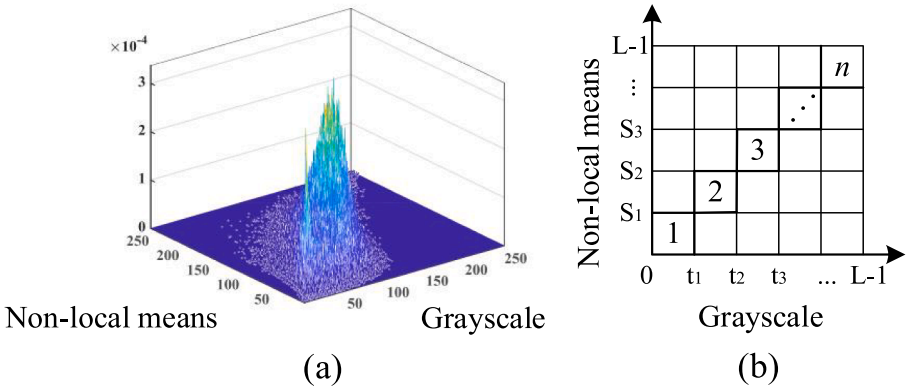

Fig. 2. The 2-D histogram and the plan view.

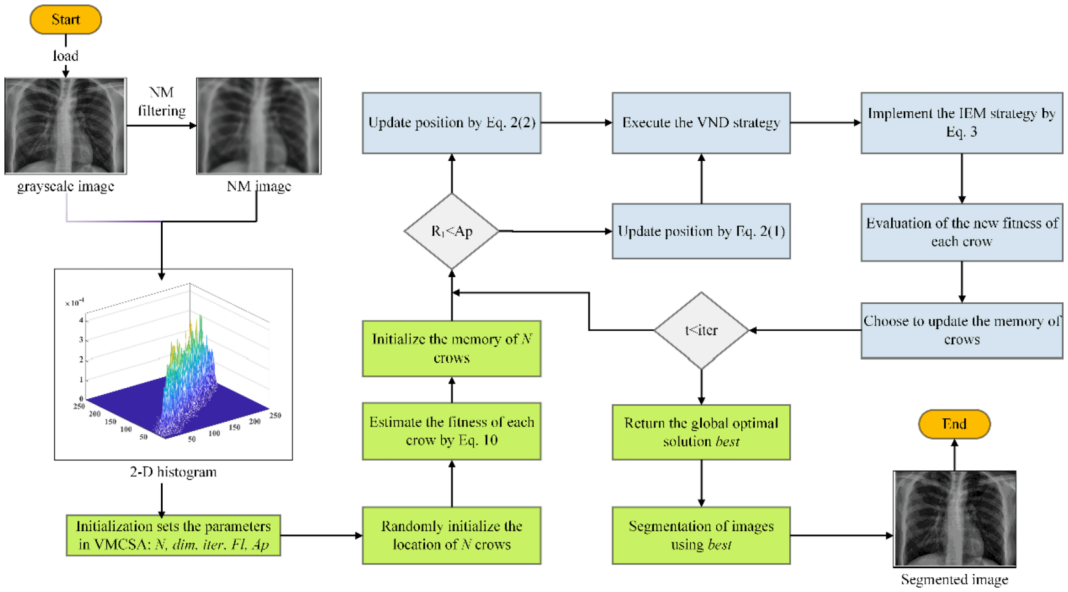

Fig. 3. Flowchart of the MTIS method based on VMCSA.

Table 2
Details of the CEC2014 function.

ID	Name of the function	Class	*Dim*	F_{min}
F1	Rotated High Conditioned Elliptic Function	Unimodal	30	100
F2	Rotated Bent Cigar Function	Unimodal	30	200
F3	Rotated Discus Function	Unimodal	30	300
F4	Shifted and Rotated Rosenbrock's Function	Multimodal	30	400
F5	Shifted and Rotated Ackley's Function	Multimodal	30	500
F6	Shifted and Rotated Weierstrass Function	Multimodal	30	600
F7	Shifted and Rotated Griewank's Function	Multimodal	30	700
F8	Shifted Rastrigin's Function	Multimodal	30	800
F9	Shifted and Rotated Rastrigin's Function	Multimodal	30	900
F10	Shifted Schwefel's Function	Multimodal	30	1000
F11	Shifted and Rotated Schwefel's Function	Multimodal	30	1100
F12	Shifted and Rotated Katsuura Function	Multimodal	30	1200
F13	Shifted and Rotated HappyCat Function	Multimodal	30	1300
F14	Shifted and Rotated HGBat Function	Multimodal	30	1400
F15	Shifted and Rotated Expanded Griewank's plus Rosenbrock's Function	Multimodal	30	1500
F16	Shifted and Rotated Expanded Scaffer's F6 Function	Multimodal	30	1600
F17	Hybrid Function 1	Hybrid	3	1700
F18	Hybrid Function 2	Hybrid	3	1800
F19	Hybrid Function 3	Hybrid	4	1900
F20	Hybrid Function 4	Hybrid	4	2000
F21	Hybrid Function 5	Hybrid	5	2100
F22	Hybrid Function 6	Hybrid	5	2200
F23	Composition Function 1	Composition	5	2300
F24	Composition Function 2	Composition	3	2400
F25	Composition Function 3	Composition	3	2500
F26	Composition Function 4	Composition	3	2600
F27	Composition Function 5	Composition	5	2700
F28	Composition Function 6	Composition	5	2800
F29	Composition Function 7	Composition	3	2900
F30	Composition Function 8	Composition	3	3000

Table 3
Details of the CEC'21 benchmark suite.

	No.	Functions	F_{min}
Unimodal Function	1	Shifted and Rotated Bent Cigar Function (CEC 2017 (Wu, Mallipeddi, Suganthan, Kyungpook National University, & Nanyang Technological University, 2017) F1)	100
Basic Functions	2	Shifted and Rotated Schwefel's Function (CEC 2014 (Liang, Qu, & Suganthan, 2013) F11)	1100
	3	Shifted and Rotated Lunacek bi-Rastrigin Function (CEC 2017 (Wu et al., 2017) F7)	700
	4	Expanded Rosenbrock's plus Griewangk's Function (CEC 2017 (Wu et al., 2017) F19)	1900
Hybrid Functions	5	Hybrid Function 1 ($N = 3$) (CEC 2014 (Liang, Qu, & Suganthan, 2013) F17)	1700
	6	Hybrid Function 2 ($N = 4$) (CEC 2017 (Wu et al., 2017) F16)	1600
	7	Hybrid Function 3 ($N = 5$) (CEC 2014 (Liang, Qu, & Suganthan, 2013) F21)	2100
Composition Functions	8	Composition Function 1 ($N = 3$) (CEC 2017 (Wu et al., 2017) F22)	2200
	9	Composition Function 2 ($N = 4$) (CEC 2017 (Wu et al., 2017) F24)	2400
	10	Composition Function 3 ($N = 5$) (CEC 2017 (Wu et al., 2017) F25)	2500
Search range: [−100,100]			

Optimization algorithm to solve the underwater IS problem, and the experimental results proved the method's effectiveness. Upadhyay and Chhabra (2020) proposed Kapur's entropy-based CSA to evaluate the optimal multi-level threshold value. The comparison results with other algorithms proved the effectiveness of the scheme. Khairuzzaman et al. [99] proposed an improved Moth Flame Algorithm and applied it to the MTIS problem to select the optimal threshold with cross entropy as the objective function. The experimental results demonstrated the superiority of the method. Luo, Yang, and Shi (2019) proposed an MTIS method for 2D Otsu based on improved adaptive DE (JADE); the proposed scheme was demonstrated to improve segmentation accuracy and speed through comparative experiments significantly. Zhou, Yang, Ling, and Zhang (2018) used Kapur's entropy-based Moth Swarm Algorithm to optimize the thresholds of the eight test images. The segmentation results show that the method has good effectiveness and robustness. Singla, Patra, and Processing (2017) proposed a context-sensitive fast threshold selection method to solve the IS problem, using the cluster validity measure to determine the optimal number of thresholds and the optimal boundaries and then using the genetic algorithm to select the optimal values. Table 1 presents a summary of these algorithms.

The above-mentioned works all use algorithms to overcome the MTIS problem of images, but there is a lack of experimental segmentation of X-ray images for COVID-19. At present, we firstly improve the threshold selection for effective segmentation of X-ray images by proposing the use of 2D histograms based on the non-local mean (NM) and gray values, which can effectively utilize the spatial information of the images, and then the extraction of thresholds by defining 2D Renyi's entropy. Our proposed VMCSA can make good use of the 2D Renyi's entropy for threshold selection. CSA has a good performance in finding the optimal value, but its mode is relatively homogeneous and can cause the problem of falling into local optimum when solving some problems. Firstly, adding the VND mechanism increases the population's diversity and improves the algorithm's probability of finding the optimal solution. Then, the IEM strategy introduced can improve the local exploitation ability of the agent and speed up the convergence ability of the population. Therefore, we are motivated to introduce these two strategies into CSA to propose a new model to overcome the MTIS problem for X-ray images of COVID-19.

3. Overview of the mentioned methods

3.1. Crow search algorithm (CSA)

Askarzadeh (2016) designed a novel metaheuristic algorithm, CSA, to find the optimal solution by simulating the foraging behavior of crows to search the search space. The crow is regarded as one of the most intelligent birds that can remember where food was hidden months ago. It will typically hide the extra food and take it out when needed. Furthermore, it will follow other crows to steal food and use its experience as a thief to prevent other crows from stealing. Suppose the whole population ((as shown in Eq. (1)) has N crows and is randomly initialized in the search space of *dim* dimension. The position of each crow i in the search space at t iterations is represented by the vector x_i^t ($t = 1,2,3\ldots iter$; $i = 1,2,3\ldots N$), *iter* refers to the maximum number of iterations. The location of the crow is updated as presented in Eq. (2) (Askarzadeh, 2016).

$$crows = \begin{bmatrix} x_1^1 & x_2^1 & \cdots & x_{dim}^1 \\ x_1^2 & x_2^2 & \cdots & x_{dim}^2 \\ \vdots & \vdots & \ddots & \vdots \\ x_1^N & x_2^N & \cdots & x_{dim}^N \end{bmatrix} \quad (1)$$

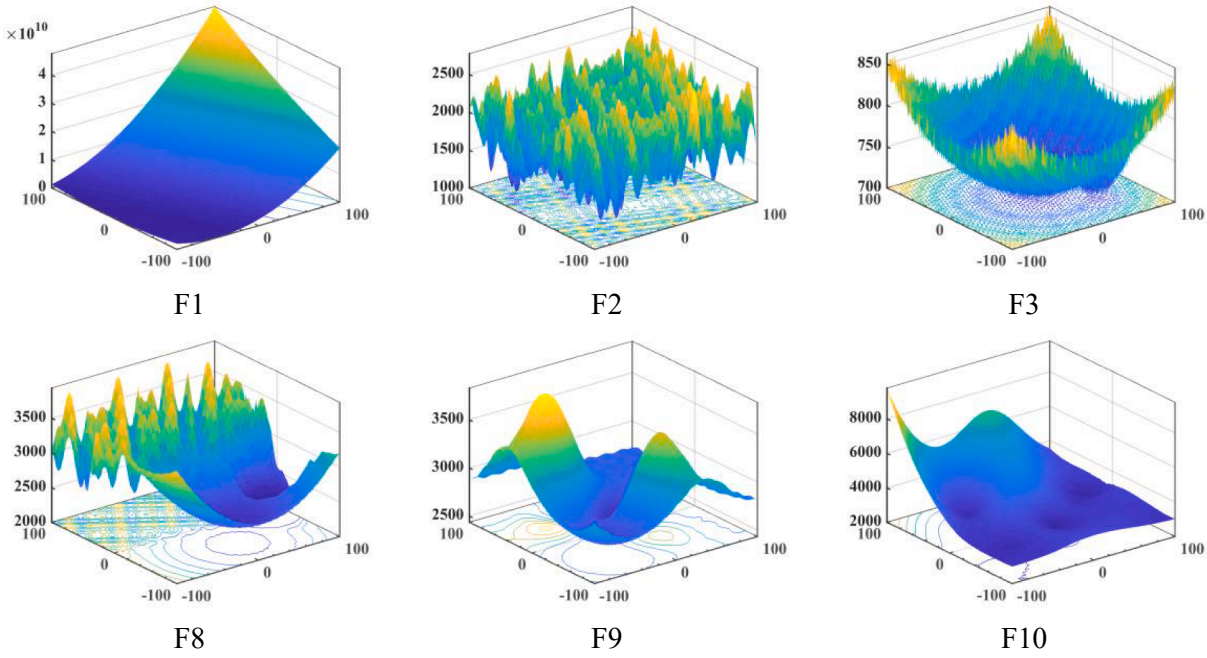

Fig. 4. Visual representation of some functions.

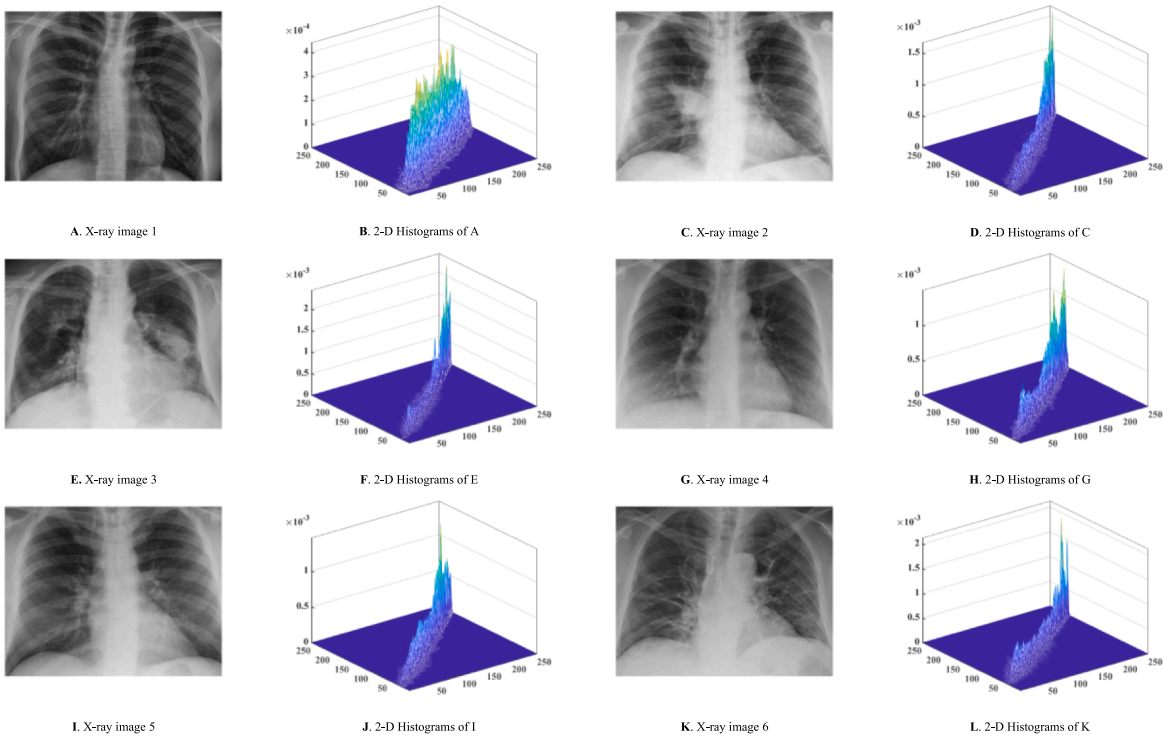

Fig. 5. X-ray images of COVID-19 and corresponding 2-D histogram.

Table 4
Different variants under the strategies.

	VND	IEM
CSA	*N*	*N*
VCSA	*Y*	*N*
MCSA	*N*	*Y*
VMCSA	*Y*	*Y*

$$x_i^{t+1} = \begin{cases} x_i^t + r \times Fl_i^t \times (me_j^t - x_i^t) r_1 \geq Ap_j^t \\ arandompositionr_1 < Ap_j^t \end{cases} \quad (2)$$

where both r and r_1 are uniformly distributed random numbers between 0 and 1.Fl_i^t refers to the flight length of the crow i at t number of iterations, which affects the exploration and exploitation ability of the algorithm.me_j^t indicates the memory location where the crow j hides its

Table 5
The p-value of Wilcoxon sign-rank tests and average ranking.

	VMCSA	VCSA	MCSA	CSA
F1	N/A	1.734E-06	2.370E-05	2.765E-03
F2	N/A	1.734E-06	3.286E-01	8.774E-01
F3	N/A	1.734E-06	1.734E-06	1.734E-06
F4	N/A	2.603E-06	5.446E-02	2.831E-04
F5	N/A	3.589E-04	2.289E-01	9.590E-01
F6	N/A	6.984E-06	9.711E-05	1.734E-06
F7	N/A	1.734E-06	8.451E-01	3.160E-02
F8	N/A	9.316E-06	2.603E-06	1.734E-06
F9	N/A	5.320E-03	9.754E-01	4.114E-03
F10	N/A	1.589E-01	1.921E-06	1.734E-06
F11	N/A	4.779E-01	3.881E-04	1.108E-02
F12	N/A	9.777E-02	1.127E-05	1.734E-06
F13	N/A	9.777E-02	7.971E-01	2.765E-03
F14	N/A	1.957E-02	5.999E-01	1.306E-01
F15	N/A	8.730E-03	2.564E-02	5.706E-04
F16	N/A	7.036E-01	1.150E-04	4.286E-06
F17	N/A	1.734E-06	5.216E-06	3.182E-06
F18	N/A	7.865E-02	9.368E-02	1.965E-03
F19	N/A	5.320E-03	1.397E-02	1.833E-03
F20	N/A	1.127E-05	6.733E-01	6.583E-01
F21	N/A	3.405E-05	5.307E-05	7.514E-05
F22	N/A	1.359E-04	2.304E-02	5.752E-06
F23	N/A	1.000E + 00	1.734E-06	1.734E-06
F24	N/A	2.712E-01	1.734E-06	1.734E-06
F25	N/A	1.000E + 00	1.734E-06	1.734E-06
F26	N/A	8.221E-02	7.189E-01	4.908E-01
F27	N/A	1.000E + 00	1.734E-06	1.734E-06
F28	N/A	1.000E + 00	1.734E-06	1.734E-06
F29	N/A	1.000E + 00	1.734E-06	1.734E-06
F30	N/A	4.048E-01	1.734E-06	1.734E-06
+/=/-	~	15/14/1	15/10/5	22/5/3
Avg	1.7	2.633333	2.566667	2.933333
Rank	1	3	2	4

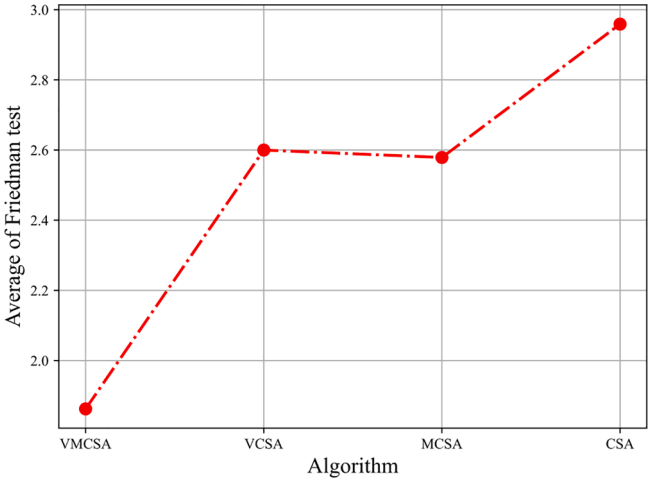

Fig. 6. The average value based on Friedman test.

food at t number of iterations.Ap_j^t represents the awareness probability of the crow j at t number of iterations.

The pseudo-code of CSA is presented as follows:

Algorithm 1: Crow Search Algorithm

Initialization sets the parameters in CSA: *N, dim, iter, Fl, Ap*;
Randomly initialize the location of *N* crows;
Estimate the fitness of each crow;
Initialize the memory of *N* crows;
While ($t < iter$)
  Randomly select a crow to follow (e.g. j).;
  For $i = 1$: N
    If ($r_1 \geq Ap_j^t$) **then**
      $x_i^{t+1} = x_i^t + r \times Fl_i^t \times (me_j^t - x_i^t)$;
    Else
      $x_i^{t+1} = arandomposition$;
    End if
  End for
  Determine if the new location of each crow is in the search space;
  Evaluation of the new fitness of each crow;
  Choose to update the memory of crows;
  Select the optimal solution *best*;
  $t = t + 1$;
End while
Return *best*.

3.2. Variable neighborhood descent (VND)

Variable neighborhood descent (VND) is an improved local search algorithm inspired by Hansen, Mladenovic, and Perez (2008). The CSA algorithm is prone to local optimum because of the fixed perceptual probability and flight length. We can use the strong local search capability of VND to compensate for the shortcomings of CSA. VND uses a neighborhood structure composed of different actions to perform alternating searches around the solution, which achieves a good balance between exploration and exploitability. The VND is illustrated in Fig. 1. VND (Zhang, Hong, & Liu, 2020) includes three neighboring institutions in this paper, which are V_1,V_2 and V_3.

Neighborhood structures are transformation functions that allow the current solution to generate its corresponding neighboring solutions. The operation of the V_1 neighborhood structure is presented as follows: Two dimensions are randomly selected from the individuals to exchange positions. The other dimensional information remains unchanged, and the new solution is obtained. For example, assume that the current individual is $x = [1,2,3,4,5,6,7,8]$. Two dimensions 3 and 6 are chosen randomly. Then the two dimensions are exchanged to obtain the new solution as $x = [1,2,6,4,5,3,7,8]$.

The operation of the V_2 neighborhood structure is described as follows: two dimensions are randomly selected from one population individual and swapped so that a new individual is generated. This process enhances the local search capability of the algorithm. For example, assume that $x = [1,2,3,4,5,6,7,8]$ is the individual of the population and randomly select two dimensions of the individual 4 and 7. The front of dimension 4 and the back of dimension 7 remain unchanged, and the dimensions between them are flipped so that a new individual $x = [1,2,3,7,6,5,4,8]$ is obtained.

The operation of the V_3 neighborhood structure is shown as follows: Three dimensions are randomly selected from an individual in the

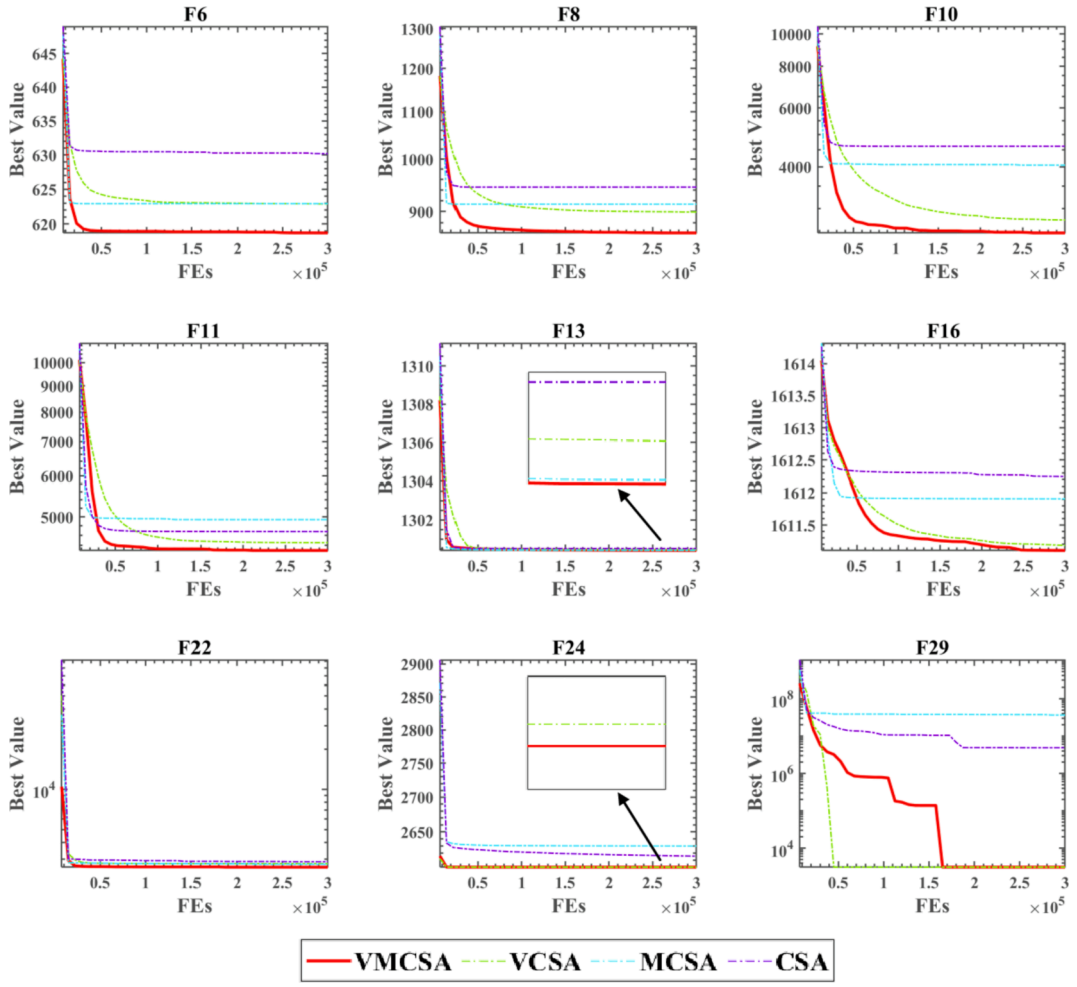

Fig. 7. Convergence curves of the four variants.

population and swapped, resulting in a new solution. For example, assume that the current individual is $x = [1, 2, 3, 4, 5, 6, 7, 8]$. Three dimensions 2,5, and 8 are randomly selected. Then the structure V_3 operations are performed on (2,5), (2,8) and (5,8), respectively. After this operation, the three solutions x_1, x_2 and x_3 can be acquired sequentially, where $x_1 = [1, 5, 4, 3, 2, 6, 7, 8]$, $x_2 = [1, 5, 4, 3, 8, 7, 6, 2]$ and new individual $x_3 = [1, 8, 3, 4, 5, 7, 6, 2]$.

The new solution obtained by VND is then diffused in steps of uniformly distributed random numbers between 0 and 1 to increase the possibility of jumping out of the local optimum.

3.3. Information exchange mutation (IEM)

The IEM strategy mutates according to the information exchange between the optimal solution and the individuals. We update the dimensionality of the population of individuals based on the random step size of crow i and the memory of crow j, and then combine it with the optimal solution to ensure the exploration of the search space and increase the possibility of the algorithm to find the optimal solution so that CSA is less likely to fall into a local optimum. The mathematical model of the method is as follows:

$$x_i^{t+1} = itrbest^t + \sigma \times (me_A^t - x_B^t) \tag{3}$$

where $itrbest^t$ is the optimal solution obtained at t iterations and σ is a matrix of 1 row dim columns, where the numbers are between 0 and 1. me_A^t refers to the memory of a random crow in the population at t iterations, and x_B^t denotes a random crow in the population.

3.4. Multi-level threshold image segmentation (MTIS) methods

3.4.1. Non-local means (NM) 2D histograms

The traditional MTIS is based on a 1D histogram for threshold selection. However, the 1D histogram of the image only considers the gray value distribution of the image without considering the spatial information of the image, noise, and other influencing factors, resulting in the histogram does not necessarily appear obvious "peaks and valleys", so the use of gray value information only often does not get satisfactory segmentation results. In recent years, many researchers have used the 2D histogram to select the threshold value, which takes into account the local information of the image on the basis of the gray value information and greatly improves the noise immunity and the accuracy of segmentation (Chon & Kim, 2006; Yimit & Hagihara, 2018).

Table 6
The p-value of Wilcoxon sign-rank tests and average ranking.

	VMCSA	SCA	m_SCA	MFO	GWO
F1	N/A	1.953E-03	1.953E-03	1.953E-03	1.953E-03
F2	N/A	1.953E-03	2.324E-01	3.711E-02	3.223E-01
F3	N/A	1.953E-03	1.953E-03	1.953E-03	6.250E-01
F4	N/A	1.953E-03	1.953E-03	5.859E-03	1.953E-03
F5	N/A	1.953E-03	1.953E-03	9.766E-03	1.953E-03
F6	N/A	1.953E-03	3.750E-01	9.766E-03	6.953E-01
F7	N/A	1.953E-03	9.766E-03	1.367E-02	1.953E-03
F8	N/A	1.953E-03	1.953E-03	1.953E-03	1.953E-03
F9	N/A	1.953E-03	8.398E-02	1.953E-03	9.219E-01
F10	N/A	1.953E-03	1.953E-03	9.766E-03	5.859E-03
+/=/-	~	10/0/0	7/3/0	10/0/0	6/4/0
Avg Rank	1.4 1	7.9 8	4.2 4	6.5 7	2.8 2

	SCADE	PSO	WOA	ACWOA	BMWOA
F1	1.953E-03	1.953E-03	1.953E-03	1.953E-03	1.953E-03
F2	1.953E-03	3.906E-03	3.906E-03	1.953E-03	1.953E-03
F3	1.953E-03	1.953E-03	1.953E-03	1.953E-03	1.953E-03
F4	1.953E-03	1.953E-03	1.953E-03	1.953E-03	1.953E-03
F5	1.953E-03	1.953E-03	1.953E-03	1.953E-03	1.953E-03
F6	1.953E-03	1.367E-02	9.766E-03	1.953E-03	5.859E-03
F7	1.953E-03	8.398E-02	1.953E-03	1.953E-03	1.953E-03
F8	1.953E-03	1.953E-03	1.953E-03	1.953E-03	1.953E-03
F9	1.953E-03	1.953E-03	1.953E-03	1.953E-03	1.953E-03
F10	1.953E-03	2.754E-01	5.859E-03	1.953E-03	1.953E-03
+/=/-	10/0/0	8/2/0	10/0/0	10/0/0	10/0/0
Avg Rank	8.5 10	3.9 3	5.9 6	8.3 9	5.6 5

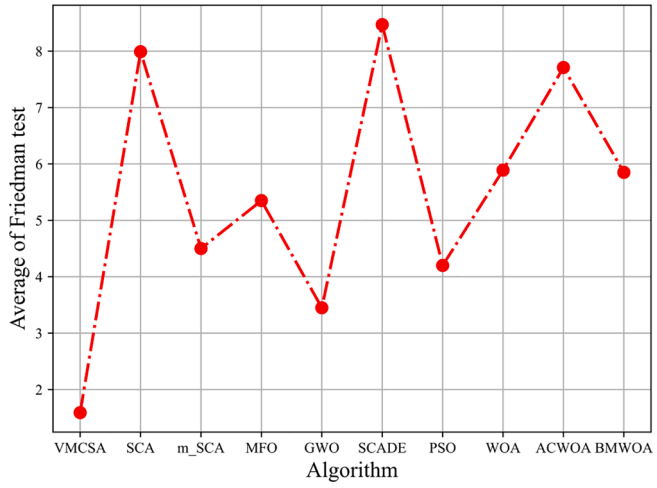

Fig. 8. The average value based on Friedman test.

In the last decade or so, denoising technologies have been rapidly developed. One of the NM proposed by Buades, Coll, and Morel (2005) has received wide attention. It is because this technique in denoising is to maximize the retention of detailed features of the image, and fully utilize the redundant information of the image. The basic idea is that the estimate of the current pixel is obtained by a weighted average of the pixels in the image that have a similar neighborhood structure to it. Suppose $g(e)$ and $g(f)$ are the grayscale values of pixels e and f in image I. Then the NM of image I is calculated as follows (Buades et al., 2005):

$$NM(e) = \sum_{f \in I} w(e,f) g(f) \tag{4}$$

$$w(e,f) = \frac{1}{U} exp \frac{-\|v(e)-v(f)\|^2}{h^2} \tag{5}$$

$$U = \sum_{f \in I} exp \frac{-\|v(e)-v(f)\|^2}{h^2} \tag{6}$$

$$v(e) = \frac{1}{n \times n} \sum_{p \in B(e)} g(p) \tag{7}$$

$$v(f) = \frac{1}{n \times n} \sum_{q \in B(f)} g(q) \tag{8}$$

where $NM(e)$ is the grayscale values of pixel e of the image after NM denoising, $w(e,f)$ refers to the corresponding weights of pixel e and f, U denotes the normalization coefficient,h refers to the control parameter, both $v(e)$ and $v(f)$ are local means.$v(e)$ means the blocks of pixels surrounding pixel e with size $n \times n$.$v(f)$ means the blocks of pixels surrounding pixel f with size $n \times n$.

The size of the grayscale image I_g of image I is $m \times n$, then the size of the NM image G obtained by NM filtering is also $m \times n$. Here a 2-D histogram is established by the grayscale image I_g and the NM image G. The points (t,s) is generated by the grayscale values of the pixels (e,f) in the grayscale image I_g and the grayscale values of the pixels (e,f) in the NM image G. So the number of occurrences of point (t,s) is represented by $T(t,s)$. The joint probability densities of the points (t,s) are obtained by Eq. (9) (Abutaleb, 1989), and using the obtained joint probability densities, we can generate a 2-D histogram as in Fig. 2(a), and Fig. 2(b) is the corresponds plan view.

$$p(t,s) = \frac{T(t,s)}{m \times n} \tag{9}$$

3.4.2. Renyi's entropy

The Renyi's entropy is a broad version of Shannon's entropy. Because it carries a positive parameter α, which makes it more adaptable to many types of images than Shannon's entropy in IS. The Renyi's entropy depends on the NM image and the grayscale image. Here let the gray level of both grayscale image I_g and NM image G be *L-1*. As shown in Fig. 2(b), the pixel gray level t and NM gray level s form an *L-1* binary group, where are $\{(t_1,s_1),(t_2,s_2),\cdots(t_{L-1},s_{L-1})\}$. So the calculation of Renyi's entropy $\delta^\alpha(t,s)$ can be described as following (Shubham & Bhandari, 2019):

$$\delta^\alpha(t,s) = H_1^\alpha + H_2^\alpha + \cdots + H_k^\alpha \tag{10}$$

$$\begin{cases} H_1^\alpha = \frac{1}{1-\alpha} \ln \sum_{e=0}^{t_1} \sum_{f=0}^{s_1} \left(\frac{p(e,f)}{P_1(t_1,s_1)} \right)^\alpha \\ P_1(t_1,s_1) = \sum_{e=0}^{t_1} \sum_{f=0}^{s_1} p(e,f) \end{cases} \tag{10.1}$$

$$\begin{cases} H_2^\alpha = \frac{1}{1-\alpha} \ln \sum_{e=t_1+1}^{t_2} \sum_{f=s_1+1}^{s_2} \left(\frac{p(e,f)}{P_2(t_2,s_2)} \right)^\alpha \\ P_2(t_2,s_2) = \sum_{e=t_1+1}^{t_2} \sum_{f=s_1+1}^{s_2} p(e,f) \end{cases} \tag{10.2}$$

⋮

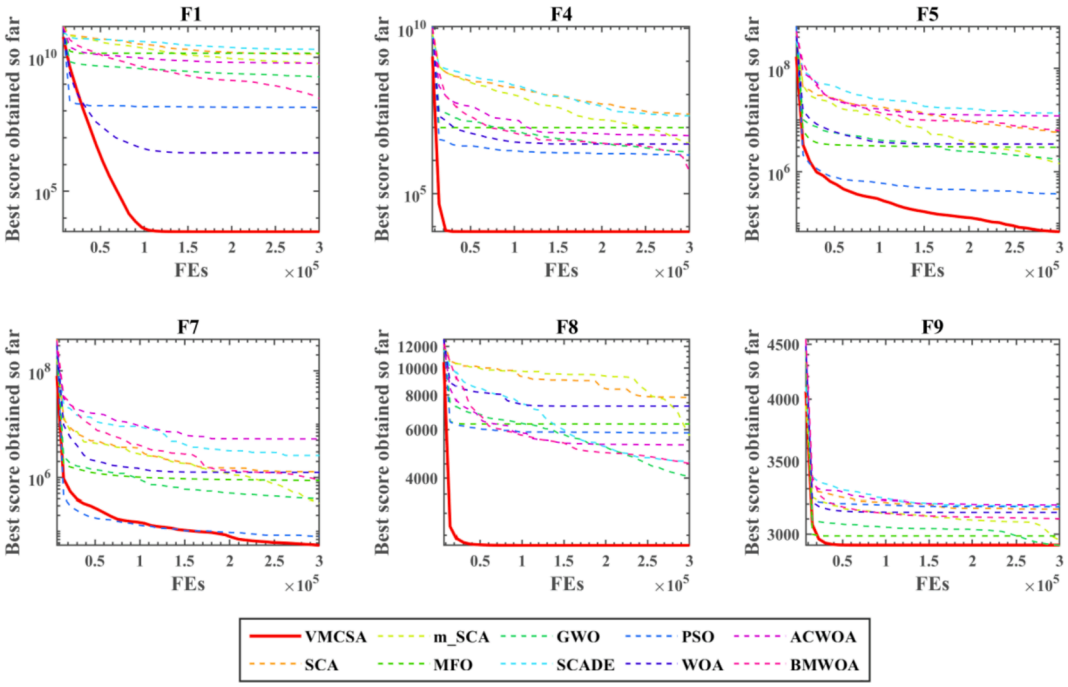

Fig. 9. Convergence curves of different algorithms.

Table 7
The Renyi's entropy of different methods.

Image	K	VMCSA	CSA	DE	HHO	PSO	CS	BLPSO	IWOA	IGWO	CGPSO
X-ray image 1	8	**58.14603**	57.86603	57.6074	57.72757	57.95008	57.11868	56.48722	57.09998	57.06334	58.02598
	10	**67.01441**	66.36654	66.11907	66.25989	66.64387	65.65337	65.45211	64.5594	65.58986	66.7344
	15	**86.28194**	85.38109	84.70875	84.58798	84.80863	84.78825	81.07983	83.01983	81.68061	85.47383
	18	**96.5043**	95.24024	93.61476	93.83096	93.71538	92.76451	90.11032	91.03587	91.93327	94.64776
	20	**102.6014**	100.8651	99.50765	99.45015	99.36931	98.42369	94.49637	95.90344	94.51445	100.0114
X-ray image 2	8	**58.03456**	57.58776	57.16534	57.14837	57.83106	56.77976	55.52849	56.2614	56.70377	57.85021
	10	**67.05878**	66.0898	66.10664	65.98995	66.42708	65.45667	63.34191	64.87049	64.99363	66.39842
	15	**86.28425**	84.82438	83.48696	83.82497	84.88815	84.08511	80.18338	81.56229	81.11301	84.95512
	18	**96.01876**	94.81752	93.4232	93.83482	94.14613	91.74921	87.36384	90.4981	89.61049	93.7317
	20	**102.2785**	99.95554	97.92748	98.72301	98.38864	98.13192	95.08749	95.76677	93.88417	99.42983
X-ray image 3	8	**57.99627**	56.81871	56.5952	57.0977	57.55346	56.84097	56.17343	55.60938	56.76565	57.7536
	10	**66.89203**	65.93189	65.94241	65.48809	66.44522	65.66165	62.90809	63.92028	64.76891	66.18871
	15	**85.96312**	85.03271	84.23659	84.42748	84.2027	83.1144	80.03942	81.10358	80.90498	84.62046
	18	**95.91492**	94.33622	93.04412	92.842	92.9041	91.45362	88.82993	89.89775	88.41518	93.37396
	20	**101.8668**	100.2852	98.21732	96.64728	98.69065	96.69925	92.76687	93.32793	91.1481	98.78109
X-ray image 4	8	**57.56417**	56.58657	56.50466	56.57915	57.22809	56.07852	54.20936	55.22522	56.41241	56.53977
	10	**66.27442**	65.47175	65.04444	65.69733	66.12604	63.99906	62.5148	63.42844	65.36627	66.20507
	15	**85.56084**	84.79084	83.46996	82.67878	84.54474	82.31245	78.34272	79.44531	80.06025	84.38209
	18	**95.5729**	93.17156	92.8877	91.53264	92.36451	91.23427	86.1507	88.71988	89.46169	93.17004
	20	**101.7286**	99.01807	97.21413	96.76491	97.77676	96.60315	90.73837	92.62269	94.12767	98.22743
X-ray image 5	8	**58.05752**	57.59143	57.77634	57.1433	57.82685	57.22994	56.45211	56.22156	56.50444	57.88464
	10	**67.01097**	66.63515	66.37356	65.42499	66.64726	65.72188	64.42224	64.28928	65.24697	66.65935
	15	**86.16045**	85.49452	84.37674	83.96198	85.00552	83.4588	81.27503	81.47797	82.11262	85.15148
	18	**96.19633**	94.92879	93.87862	92.22865	93.68277	93.22863	89.82034	90.86623	88.95482	94.06742
	20	**102.2288**	100.8846	98.76399	98.11936	99.62763	98.21476	94.51719	97.18698	95.7369	99.51077
X-ray image 6	8	**57.80078**	56.77248	57.0821	56.8815	57.28241	56.55121	55.77338	55.69244	56.35904	57.35387
	10	**66.78789**	66.49583	66.20196	65.03599	66.23554	64.99424	64.49335	64.30335	64.62624	66.2928
	15	**86.22567**	85.35202	83.86634	83.36277	84.80855	82.57354	80.468	81.9491	80.16618	84.92957
	18	**96.03381**	95.33836	93.35581	92.74782	93.50132	91.80394	88.04698	92.07018	88.98718	93.67182
	20	**102.3671**	101.1836	99.77337	99.32414	99.33093	98.01054	93.33528	94.73884	92.68168	99.15955

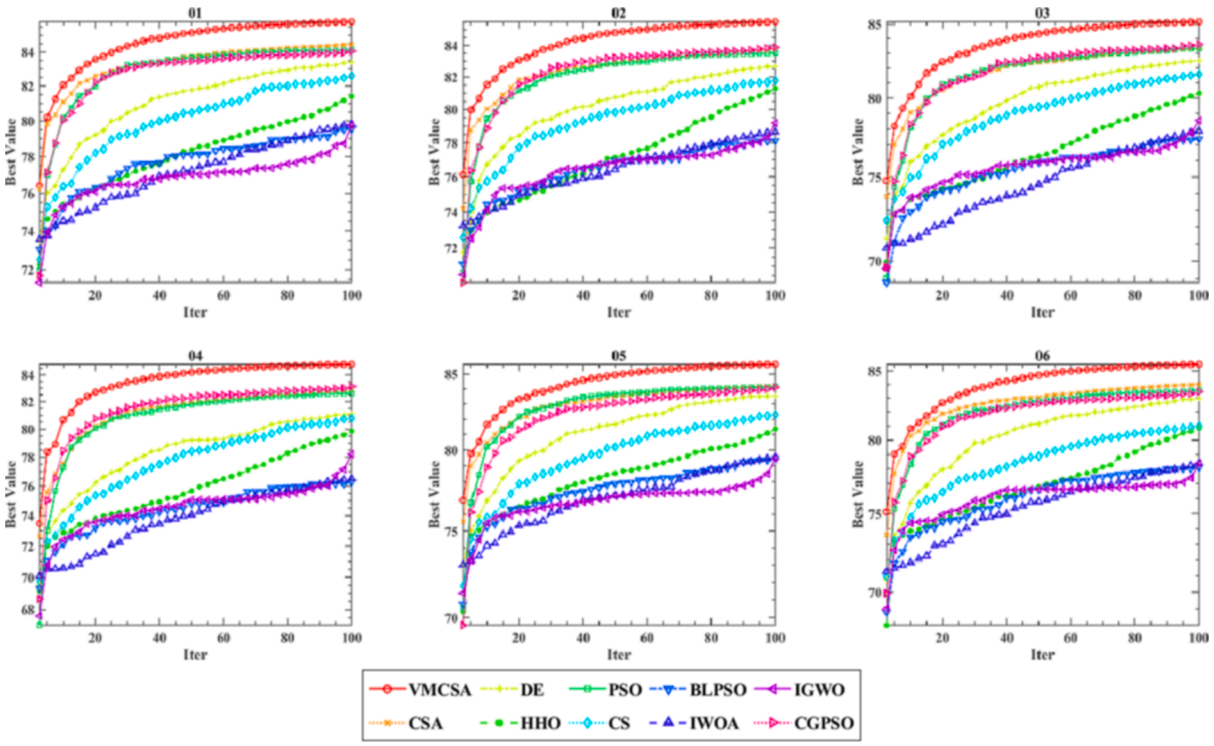

Fig. 10. The convergence curves of Renyi's entropy at the threshold level of 15.

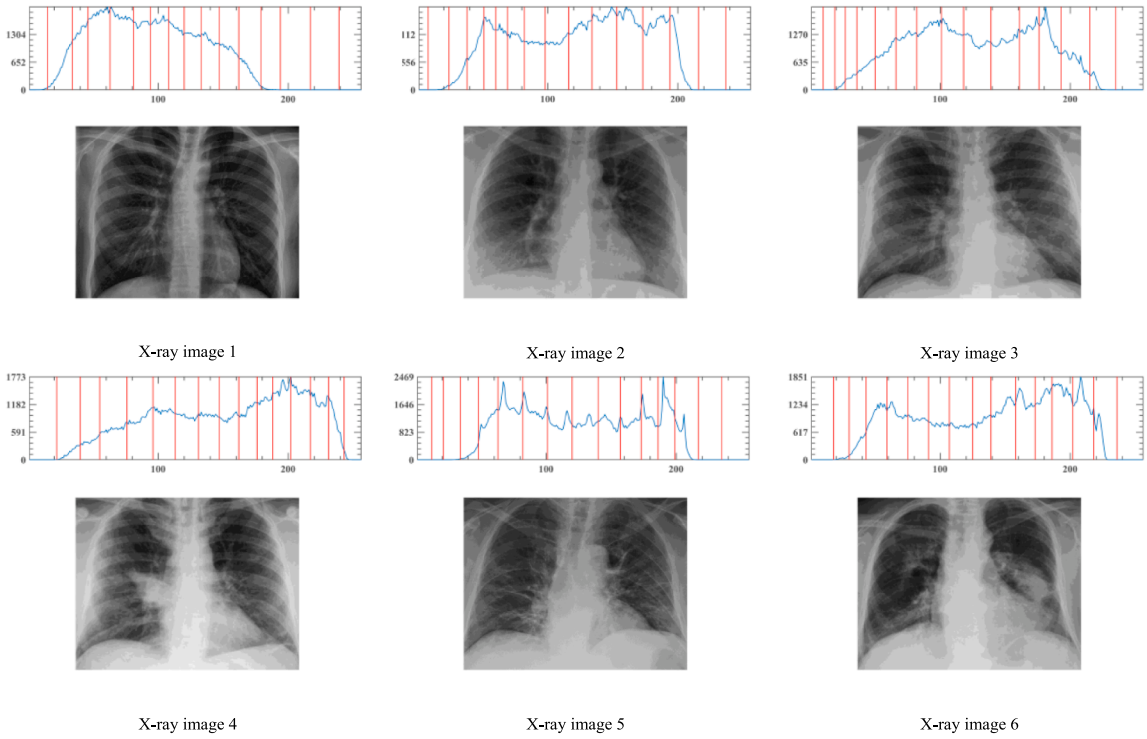

Fig. 11. Thresholds and segmented images obtained by the proposed segmentation algorithm on the histogram of all test images at the threshold level of 15.

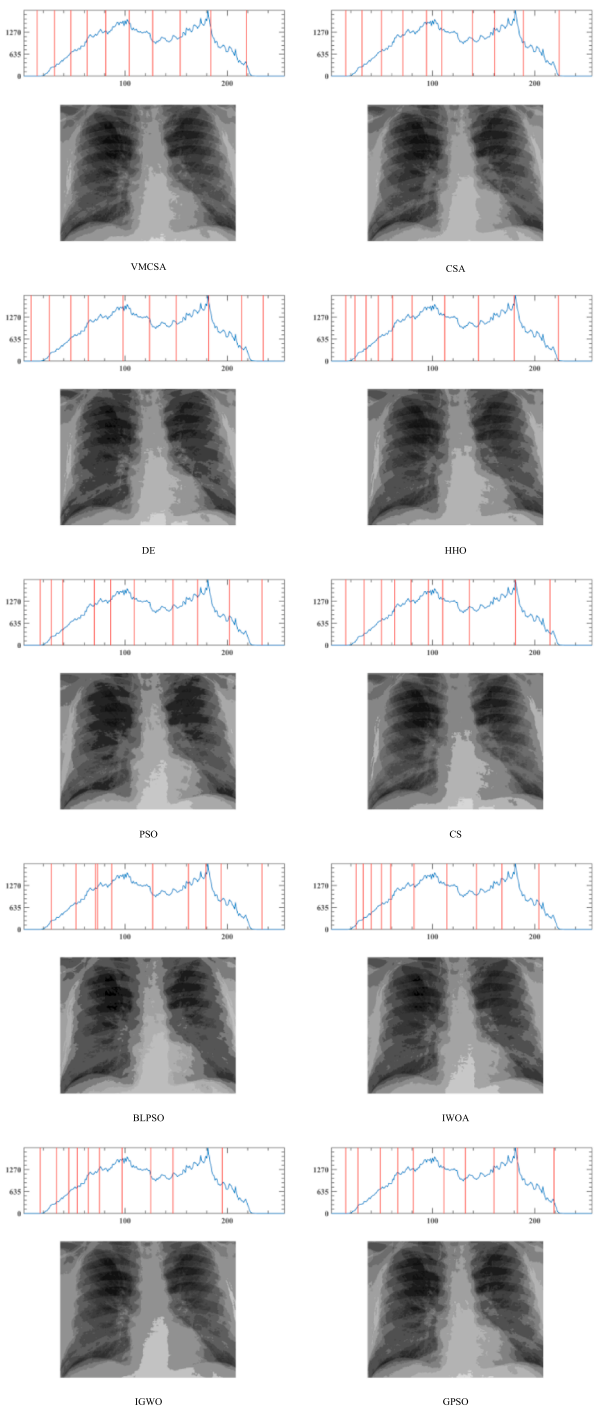

Fig. 12. Thresholds and segmented images obtained by different segmentation algorithms on the histogram of the X-ray image 3 at the threshold level of 10.

$$\begin{cases} H^{\alpha}_{L-1} = \dfrac{1}{1-\alpha}\ln\sum_{e=t_{L-2}+1}^{t_{L-1}}\sum_{f=s_{L-2}+1}^{s_{L-1}}\left(\dfrac{p(e,f)}{P_k(t_{L-1},s_{L-1})}\right)^{\alpha} \\ P_{L-1}(t_{L-1},s_{L-1}) = \sum_{e=t_{L-2}+1}^{t_{L-1}}\sum_{f=s_{L-2}+1}^{s_{L-1}}p(e,f) \end{cases} \tag{10.L-1}$$

Take Renyi's entropy as the fitness function of the proposed algorithm. Therefore, the set $\{t_1, t_2, \cdots t_{L-1}\}$ is the chosen optimal threshold by setting the binary groups $\{(t_1, s_1), (t_2, s_2), \cdots (t_{L-1}, s_{L-1})\}$ such that F is maximized.

4. The proposed methods

4.1. The improved CSA (VMCSA)

CSA, as a kind of MAs, has a strong space exploration capability. However, because of its fixed awareness probability (*Ap*) and flight length (*Fl*), it makes CSA easy to fall into the local optimum. The crow search mode is relatively single, which makes it unable to find the global optimal local solution effectively when solving complex problems (Qu & Fu, 2019). Moreover, introducing the VND strategy in the original CSA increases the possibility of the algorithm jumping out of the local optimum and finding the global optimal solution. The original CSA uses random individuals and random probabilities at the position update to increase the diversity of the population. However, it neglects the role of optimal solutions in population evolution, thus leading to issues such as slow convergence and premature convergence in solving complex problems. In contrast, the IEM strategy updates the individual positions by the optimal solution, which makes the optimal solution play a certain leading most use in the process of population evolution, and the diversity of the population is not reduced because of the communication between individuals. So that the convergence speed of the algorithm in dealing with multidimensional problems is improved to some extent and the premature phenomenon is avoided. **Algorithm 2** shows the pseudo-code of VMCSA.

Algorithm 2: The pseudo-code of VMCSA

Initialization sets the parameters in CSA: *N, dim, iter, Fl, Ap*;
Randomly initialize the location of *N* crows;
Estimate the fitness of each crow;
Initialize the memory of *N* crows;
While ($t < iter$)
  Randomly select a crow to follow (e.g. *j*);
  For $i = 1$: *N*
    If ($r_1 \geq Ap_j^t$) **then**
      $x_i^{t+1} = x_i^t + r \times Fl_i^t \times (me_j^t - x_i^t)$;
    Else
      $x_i^{t+1} = arandomposition$;
    End if
  End for
  Evaluate the fitness values of new crows;
  Update the population and current optimal solutions $itrbest^t$.
  For $i = 1$: *N*
    /* Execute the VND strategy */
    $K = 1$;
    While ($K \leq 3$)
      The neighborhood structure *S* is generated through V_k.
      If (The fitness value of *S* is preferred over x_i)
        x_i=*S*;
      Else
        $K = K + 1$;
      End if
    End While
    /* Implement the IEM strategy*/
    $x_i^{t+1} = itrbest^t + \sigma \times (me_A^t - x_B^t)$;
  Evaluate the fitness values of new crows and update the population;
  End for
  Determine if the new location of each crow is in the search space;
  Evaluation of the new fitness of each crow;
  Choose to update the memory of crows;
  Select the global optimal solution *best*;
  $t = t + 1$;
End while
Return *best*.

4.2. The VMCSA-based MTIS method

MTIS is used to segment an image's target and background regions by selecting multi-level thresholds and then using these thresholds. The goodness of the segmentation depends on the selection of multi-level thresholds. However, traditional methods have a large time complexity in the multi-level thresholding problem. To better implement MTIS, we use the maximum Renyi's entropy based on VMCSA to

identify the best multi-level thresholds. In addition, the 1-D histogram-based thresholding has been disturbed by noise, while the 2-D histogram based on the local mean does not make sufficient use of the whole image and the denoising effect is not satisfactory (Kim, Choi, Park, & Ko, 2016; Kumar, Vig, Varshney, & Bansal, 2020; Mittal & Saraswat, 2018). Therefore, the proposed MITS method is based on an NM 2D histogram. The proposed method was also applied to the segmentation of X-ray images of COVID-19, and the operation procedure is shown in Fig. 3.

5. Experimental results and discussion

In this section, three main experiments are included: a comparison experiment on whether the effect of the proposed strategy on CSA is positive, a performance validation experiment of the proposed variant VMCSA, and an experiment on MTIS based on VMCSA. The first two experiments were experiments done at CEC2014, while the MTIS experiment was based on six X-ray images of COVID-19. And all the experiments in the paper were run on MATLAB R2018b on a Windows 10 computer, 8 GB RAM and a Core i7 CPU.

5.1. Experimental setting

The CEC2014 in the experiment is shown in detail in Table 2. The CEC2014 was divided into four types of functions, which are unimodal function (F1-F3), multimodal function (F4-F16), hybrid function (F17-F22), and composition function (F23-F30). In the first experiment, to verify the effects of VND and IEM on the original CSA, three variants were generated using two strategies as VCSA, MCSA and VMCSA, respectively, and then subjected to comparison tests. This is followed by the performance validation experiments of VMCSA by comparing it with some eminent algorithms at CEC2014, which include SCA (Mirjalili et al., 2019), m_SCA (Gupta & Deep, 2019), MFO (Mirjalili et al., 2019), GWO (Mirjalili et al., 2019), SCADE (Nenavath & Jatoth, 2018), PSO (Mirjalili et al., 2019), WOA (Mirjalili et al., 2019), ACWOA (Elhosseini, Haikal, Badawy, & Khashan, 2019) and BMWOA (Heidari, Aljarah et al., 2019). To ensure the relative fairness of the experiments, the comparison of algorithms in both sets of experiments is performed under the same circumstances. Here the maximum number of iterations is set to 300,000, the number of independent runs of each algorithm is 10, and the population size is 30. In addition, the results of the experiments are analyzed and ranked by Wilcoxon sign-rank test (García, Fernández, Luengo, & Herrera, 2010) and Friedman test (Alcalá-Fdez et al., 2009). The optimization methods have been validated based on fair comparison rules as per suggested by other related works (Liu et al., 2021; Lv, Yu, Xie, & Alamri, 2022; Wu et al., 2021).

To verify the optimization performance and applicability of the proposed algorithm, we chose to conduct comparative experiments in the CEC'21 benchmark suite. The CEC'21 benchmark suite in the experiment is shown in detail in Table 3. The experimental setting for this section remains the same as in the previous section, where the comparison algorithm parameter settings are also presented in Appendix 1. Fig. 4 is a visual display of some of these functions.

The final experiment is based on the MTIS experiment of VMCSA to segment six X-ray images of COVID-19, which were obtained from the publicly available dataset collection of Cohen *et al.* (Cohen et al., 2020). Fig. 5 illustrates the chosen images (512×400) and their corresponding 2-D histograms. In order to demonstrate the superior performance of the proposed method in the MTIS problem, a comparison experiment with CSA-based (Upadhyay & Chhabra, 2020), DE-based (Storn & Price, 1997), HHO-based (Heidari, Mirjalili et al., 2019), PSO-based (Kennedy & Eberhart, 1995), CS-based (Gandomi, Yang, & Alavi, 2013), BLPSO-based (Chen, Tianfield, Mei, Du, & Liu, 2017), IWOA-based (Tubishat, Abushariah, Idris, & Aljarah, 2019), IGWO-based (Cai et al., 2019), and CGPSO-based MTIS methods will be conducted here. Furthermore, to prove the algorithm's applicability, five sets of experiments were conducted with threshold levels set to 8,10,15,18,20, respectively. Moreover, in these experiments, the population size was set to 20, the maximum number of iterations was 100, and the number of independent runs of the algorithm was 20. Finally, the experimental results were evaluated using three image quality metrics, and the results were statistically analyzed using the Friedman test.

5.2. Parameters setup

The parameters in MAs have a certain effect on the performance of the algorithms. Therefore, in order to make the experimental results more convincing, the parameters of the algorithms we used are consistent with those in the corresponding papers, and in Appendix A.1 gives the detailed settings of all the parameters of the algorithms in the experiment.

5.3. The impact of VND and IEM strategies.

The two strategies in the paper were introduced into the original CSA separately, and the combined results are given in Table 4. '*Y*' indicates that the CSA is improved using the strategy, while '*N*' means that the strategy did not improve the CSA.

Appendix A.2 shows the results of the comparison of the variants on the CEC2014 function set. The results of 30 independent runs of algorithms are analyzed in the table by average and standard deviation, where '*Avg*' indicates the average and the standard deviation is denoted by '*Std*', where the bolded one is the best performing solution.

From the data in table Appendix A.2, we can see that VMCSA does not achieve the best performance in any of the unimodal functions but is still stronger than CSA in terms of search performance, indicating that VMCSA still has good search potential. In the multimode function, VMCSA can find the optimal solution in the search space in F6-F16, and the search result is significantly better than other variants, and the results are quite optimistic, although the best results are not obtained in the F4 and F5 functions tested. Hence, VMCSA shows excellent ability to jump out of local optimum. In the hybrid function, the VMCSA performs poorly, and the best results are obtained only in the F22, which is the direction of our subsequent work to enhance the robustness of the VMCSA. In the competitive functions, VMCSA achieves outstanding computational results, all of which obtain the best solutions and show excellent performance in finding the best. It is proved that the two strategies effectively help the algorithm to avoid falling into local optimum and enhance the exploration and exploitation capability of the algorithm.

Table 5 presents the p-value of Wilcoxon sign-rank tests and average ranking. The assumptions have been judged to be valid according to the p-value, if p is greater than 0.05, it means that there is no significant difference between the two algorithms in the experiment, while the other way around. Where '-' in the table indicating that the performance of the proposed algorithm is inferior to that of the comparison algorithm, then '+' in the table indicating that the proposed algorithm is much better than the comparison algorithm, and '=' indicates that the performance of the proposed algorithm is similar to the comparison algorithm. The results from the table show that VMCSA outperforms other variants compared in the CEC2014 functions which are 15 (VMCSA vs VCSA), 15 (VMCSA vs MCSA), 22 (VMCSA vs CSA), respectively. So the proposed two strategies are effective for the improvement of CSA.

The average value based on Friedman test in Fig. 6 further reflects that the performance of the proposed algorithm VMCSA has been greatly improved. Fig. 7 shows the convergence curves of algorithms on some functions, from which we can see more graphically that the convergence speed and accuracy of the proposed algorithm have been greatly improved. Therefore, combining VDN and IEM into CSA ensures that the algorithm approaches the optimal solution stably.

5.4. Comparison in the CEC'21 benchmark suite

To further show the optimization capability and robustness of the proposed algorithm. We test the algorithm VMCSA by CEC'21. The chosen comparison algorithm include SCA (Mirjalili et al., 2019), m_SCA (Gupta & Deep, 2019), MFO (Mirjalili et al., 2019), GWO (Mirjalili et al., 2019), SCADE (Nenavath & Jatoth, 2018), PSO (Mirjalili et al., 2019), WOA (Mirjalili et al., 2019), ACWOA (Elhosseini et al., 2019) and BMWOA (Heidari, Aljarah et al., 2019). Appendix A.3 shows the results of the comparison of different algorithms on the CEC2014 function set. The results of 30 independent runs of algorithms are analyzed in the table by average (Avg) and standard deviation (Std). The optimal data has been bolded and it can be seen that the algorithm achieves the best results in most cases.

From the data in table Appendix A.3, we can see that in the unimodal function, VMCSA displays an absolute advantage with respect to the compared algorithms. VMCSA took second place in F2 and obtained the best solution on the other two functions in basic functions. The same is true on the hybrid functions, where the best solution is acquired on two functions and the second best solution is acquired on F6. In the competition functions, VMCSA does not perform as well as the above, only achieving the best search in F8, and weaker than GWO and PSO in F9 and F10, respectively, but without significant differences. The results demonstrate that VMCSA also performs strongly in the CEC'21 benchmark test set, with good robustness and convergence.

Table 6 presents the p-value of Wilcoxon sign-rank tests and average ranking. According to the statistical test analysis, if the p-value is not greater than 0.05, then the difference between the two algorithms in the experiment is significant. Otherwise, the opposite is true. Where '-' in the table indicates that the two algorithms are significantly different and performance of the proposed algorithm is inferior to that of the comparison algorithm, then '+' in the table indicates that the two algorithms are significantly different and proposed algorithm is much better than the comparison algorithm, and '=' indicates that there is no significant difference between the two algorithms. From the results in the table, we can obtain that the number of functions in which VMCSA outperforms other MAs on CEC'21 functions are 10 (VMCSA vs SCA), 7 (VMCSA vs m_SCA), 10 (VMCSA vs MFO), 6 (VMCSA vs GWO), 10 (VMCSA vs SCADE), 8 (VMCSA vs PSO), 10 (VMCSA vs WOA), 10 (VMCSA vs ACWOA), and 10 (VMCSA vs BMWOA), respectively. It can be seen that with the introduction of VND and IEM, the proposed algorithm is able to strike a better balance between exploration and exploitation, increasing the possibility of the algorithm finding the optimal solution. It shows that VMCSA outperforms SCA, m_SCA, MFO, GWO SCADE, PSO, WOA, ACWOA and BMWOA in the CEC'21 benchmark suite, and it is observed that VMCSA does not perform worse than any of the algorithms or variants in this test set. The average ranking value of the tests shows that it outperforms the other comparative algorithms and also proves that the proposed algorithm has good robustness.

Fig. 8 shows the mean values obtained based on the Friedman statistical test, and it can be seen that the proposed algorithm has the lowest ranking, which is much better than the ranking of the other algorithms, proving that the proposed algorithm is more outstanding than the other compared MAs. It is imperative to investigate the convergence behavior of the iterative methods and observe which one has a healthier rapidity in exploring more suitable solutions (Fan, Zhang, & Huang, 2022; Zhou, Fan, Huang, & Liu, 2022). Fig. 9 shows the curve convergence of VMCSA with other comparative algorithms for unimodal, basic, hybrid and composition functions on CEC'21. VMCSA displays strong convergence speed and search capability in all these different functions. In the competition function F9, the search ability of VMCSA is somewhat poor, but it is also in the leading position, and its convergence ability is still very strong.

Therefore, by analyzing the experimental results in CEC'21, VMCSA has superior performance compared with other well-known metaheuristics, and it is further demonstrated that the two strategies introduced can effectively enhance CSA and improve the algorithm's search capability and robustness.

5.5. MTIS experiment on the X-ray images of COVID-19

This section demonstrates the performance of the proposed algorithm VMCSA on MITS by comparing the experiments with the original CSA and some well-known algorithms. The fitness function evaluates the performance of the proposed algorithm and three image quality metrics (peak signal-to-noise ratio (PSNR) (Huynh-Thu & Ghanbari, 2008), structural similarity index (SSIM) (Wang, Bovik, Sheikh, & Simoncelli, 2004) and feature similarity index (FSIM) (Zhang, Zhang, Mou, & Zhang, 2011)) are used to estimate the segmented images.

5.5.1. Performance evaluation criteria

It is crucial to measure the performance of image processing works using well-defined metrics (Cao et al., 2022; Liu et al., 2022; Wang, Chen, & Yuan, 2022; Zhang et al., 2022). It is necessary for the evaluation of the segmented images. In this paper, we use the metrics PSNR, SSIM and FSIM to evaluate the segmented images; when the evaluation method has the maximum value, it means that the method has the best segmentation effect. Moreover, we also analyze the evaluation results acquired by PSNR, SSIM, and FSIM using the Friedman test method. These methods are simply defined as follows:

PSNR is used to evaluate the difference between the segmented image and the original image using the Mean Square Error (MSE) of the pixels in the image. PSNR and MSE are defined below:

$$PSNR = 10 \times log_{10}\left(\frac{255^2}{MSE}\right) = 20 \times log_{10}\left(\frac{255}{\sqrt{MSE}}\right) \tag{11}$$

$$MSE = \frac{1}{m \times n}\sum_{i=0}^{m-1}\sum_{j=0}^{n-1}\|I(i,j) - G(i,j)\|^2 \tag{12}$$

where $I(i,j)$ and $G(i,j)$ are the pixel grayscale values of the original image and the segmented image, respectively.

SSIM is also used here to compare the similarity of the original image to the segmented image, which is presented following:

$$SSIM = \frac{(2\mu_I\mu_G + c_1)(2\sigma_{I,G} + c_2)}{(\mu_I^2 + \mu_G^2 + c_1)(\sigma_I^2 + \sigma_G^2 + c_2)} \tag{13}$$

where μ_I is the average of the original image I and μ_G is the average of the segmented image G, σ_I and σ_G represent the standard deviation of I and G, respectively. While c_1 and c_2 that are two constants.

FSIM is another quality measure in the paper, revealing the local structure's importance. Phase consistency (PC) is used to depict the structure of the image, while the contrast distortion of the image is described using gradient magnitude (GM). FSIM is presented following:

$$FSIM = \frac{\sum_{X\in\Omega} S_L(X)PC_m(X)}{\sum_{X\in\Omega} PC_m(X)} \tag{14}$$

$$S_L(X) = S_{PC}(X)S_{GM}(X) \tag{14.1}$$

$$PC_m(X) = Max(PC_1(X), PC_2(X)) \tag{14.2}$$

$$S_{PC}(X) = \frac{2PC_1(X)PC_2(X) + T_1}{PC_1^2(X)PC_2^2(X) + T_1} \tag{4.1.1}$$

$$S_{GM}(X) = \frac{2GM_1(X)GM_2(X) + T_2}{GM_1^2(X)GM_2^2(X) + T_2} \tag{14.1.2}$$

$$GM = \sqrt{GM_x^2 + GM_y^2} \tag{14.1.2.1}$$

where Ω is the space field of the whole image, T_1 and T_2 refer to two constants.

5.5.2. Experimental results and analysis

This section discusses and analyzes the results of the proposed method in the MTIS problem. All the algorithms mentioned in this section use 2D Renyi's entropy as the objective function to optimally find the optimal threshold to segment the X-ray image of COVID-19 and extract the features of interest to assist the physician in making the correct diagnosis.

Appendix A.4-A.6 show the evaluation of all algorithmic segmentations by three quality metrics. We have followed fair comparison rules also for these cases (Cai, Xiong, Cao, Zhang, & Alsaadi, 2022; Xu et al., 2020; Zhou, Wang, & Wan, 2022). The data in the table represents the average and standard deviation. We can see by the bolded solution that the proposed method has the maximum average and minimum standard deviation in most cases. It is proved that the proposed algorithm VMCSA has a better performance of finding the best and robustness and can effectively avoid falling into local optimum.

The algorithm's objective function, which is the maximum Renyi's entropy obtained, is shown in Table 7. We can find from the table that the proposed algorithm VMCSA obtains the maximum Renyi's entropy at different threshold levels, which shows the excellence of the algorithm in finding the optimal threshold in MITS and the optimal solution obtained is more convincing. To clarify the results, we show in Fig. 10 the convergence curves of the maximum Renyi's entropy obtained by each method at the threshold level of 15.

We analyze the three evaluation results for PSNR, SSIM and FSIM based on the Friedman test, and Appendix A.7 shows the average results obtained at different threshold levels. The table shows that the mean value obtained by the proposed segmentation method is the maximum based on the Friedman test. This shows that the method has a better performance in the MTIS problem.

Presented in Fig. 11 is the best thresholds and segmented images obtained by the proposed segmentation algorithm in the experiments at 15 threshold levels. As the threshold level increases, the problem's dimensionality becomes larger, leading to a larger complexity, which can be demanding for the algorithm's performance. The results clearly show that our proposed method is still very competitive at high dimensionality.

The best thresholds and segmented images obtained by different segmentation algorithms at 10 threshold levels for the experiment of X-ray image 3 are shown in Fig. 12. The analysis of optimal thresholds and segmentation results can further prove that the proposed VMCSA-based MTIS method has better adaptability for different threshold levels and can obtain better segmentation results. Having better processing results at high threshold levels indicates that our improved algorithm can better find the global optimum and avoid falling into the local optimum when dealing with high latitude problems.

In addition, based on so excellent results, it is no doubt that the potential capability of the proposed method will lead to its application in many more fields, such as human motion capture (Qiu, Zhao et al., 2021), kayak cycle phase segmentation (Qiu, Hao et al., 2021), information retrieval services (Wu, Li et al., 2020; Wu, Shen, Lian, Su, & Chen, 2020; Wu, Shen et al., 2021), location-based services (Wu, Li et al., 2021; Wu, Wang, Li, Lian, & Xu, 2020), text clustering (Guan et al., 2020), recommender system (Li, Chen, Chen, & Tong, 2017; Li, Zheng, Chen, Song, & Chen, 2014; Li & Lin, 2020; Wang, Liang, Xu, Feng, & Guan, 2018), image-to-image translation (Zhang et al., 2022), image dehazing (Zhang, Wang, Wang, & Jiang, 2021), power flow optimization (Cao, Wang, & Zeng, 2022), medical image augmentation (Chen et al., 2022; Guan et al., 2022), dynamic module detection (Li, Zhang, & Ma, 2021; Ma, Sun, & Gong, 2020), disease prediction (Li et al., 2021; Su, Li, Zheng, & Zhang, 2019; Wu et al., 2021), pharmacoinformatic data mining (Yin et al., 2020; Zhu et al., 2012), microgrids planning (Cao, Sun, Xu, Zeng, & Guan, 2021), and road network planning (Huang et al., 2022).

6. Conclusions and future works

In this work, we have derived VMCSA, a variant of the original CSA that introduces two strategies, VND and IEM, to improve the algorithm's local and exploitation capabilities, enhance the algorithm's convergence, and increase the possibility of finding the optimal solution. First, we have compared experiments with nine well-known MAs at CEC2014 and CEC'21 to test the improved algorithms' performance and verify the excellence of VMCSA in the optimization domain. After that, we applied the proposed algorithm to the MTIS problem for X-ray images of COVID-19. The proposed segmentation method uses grayscale images and NM images to form a 2-D histogram and maximizes Renyi's entropy on the 2D histogram to obtain the best threshold values. The experimental results have been analyzed using fitness values and image quality metrics, PSNR, SSIM, and FSIM. The results indicated that the proposed algorithm has better segmentation than other comparative algorithms.

In the future, we will try to apply the proposed improved algorithm to more medical disease diagnosis models to contribute to disease diagnosis. We will also try to apply the proposed method to other fields for testing, such as engineering and feature selection. We will keep improving the algorithm and try to replace more objective functions, such as Otsu and Kapur's entropy.

CRediT authorship contribution statement

Songwei Zhao: Writing – original draft, Writing – review & editing, Software, Visualization, Investigation. **Pengjun Wang:** Conceptualization, Methodology, Formal analysis, Investigation, Writing – review & editing, Funding acquisition, Supervision. **Ali Asghar Heidari:** Writing – original draft, Writing – review & editing, Software, Visualization, Investigation. **Xuehua Zhao:** Writing – original draft, Writing – review & editing, Software, Visualization, Investigation. **Huiling Chen:** Conceptualization, Methodology, Formal analysis, Investigation, Writing – review & editing, Funding acquisition, Supervision.

Declaration of Competing Interest

The authors declare that they have no known competing financial interests or personal relationships that could have appeared to influence the work reported in this paper.

Data availability

Data will be made available on request.

Acknowledgments

This research is supported by the Zhejiang Provincial Natural Science Foundation of China (LJ19F020001), Science and Technology Plan Project of Wenzhou, China (2018ZG012), and National Natural Science Foundation of China (62076185, 71803136), Guangdong Natural Science Foundation (2018A030313339) and Scientific Research Team Project of Shenzhen Institute of Information Technology (SZIIT2019KJ022).

Appendix A

See .

Appendix A.1

Parameter settings for all algorithms in the experiment.

Algorithms	Parameters	Values
VMCSA	awareness probability (*Ap*)flight length	0.1
	(*Fl*)Neighborhood structure	2
	(*K*)	3
SCA	Constant (*a*)	2
m_SCA	Constant (*a*)jumping rate	2
	(JR)self-adaptation rate	0.1rand
	(SR)	()
MFO	Constant (*b*)Decreasing coefficient	1
	(*a*)	[−1, −2]
GWO	Decreasing coefficient (*a*)	[2, 0]
SCADE	Scale factor upper and lower boundsCrossover Probability	0.8, 0.2
	(*pCR*)Constant	0.2
	(*a*)	2
PSO	Constant (*w*)	1
WOA	Decreasing coefficient (*a*)Decreasing coefficient	[2, 0]
	(a_2)	[−1, −2]
ACWOA	Decreasing coefficient (*a*)Decreasing coefficient	[2, 0]
	(a_2)Weighting parameters	[−1, −2]
	(*w*)	0.5 + 0.5*rand()
BLWOA	*N*-operator probability (bw)B-operator probability	0.001
	(Beta)Decreasing coefficient	0.1
	(*a*)Decreasing coefficient	[2, 0]
	(a_2)	[−1, −2]
CSA	awareness probability (*Ap*)flight length	0.1
	(*Fl*)	2
DE	Scale factor upper and lower boundsCrossover Probability	0.8, 0.2
	(*pCR*)	0.2
HHO	Decreasing coefficient (*a*)	[2, 0]
CS	Discovery rate (*pa*)Constant	0.25
	(*beta*)	1.5
BLPSO	Constant (*c*)	1.49445
IWOA	Crossover Probability (*CR*)Constant	0.1
	(*b*)	1
IGWO	Constant (*beta_num*)Constant	10
	(*omega_num*)	15
CGPSO	Constant (*w*)	1

Appendix A.2

Results of the proposed variants over average and standard deviation on CEC2014.

	F1		F2		F3	
	Avg	*Std*	*Avg*	*Std*	*Avg*	*Std*
VMCSA	1.396E + 06	8.751E + 05	9.531E + 03	**7.606E + 03**	4.024E + 02	1.093E + 02
VCSA	1.131E + 07	4.737E + 06	2.109E + 05	9.141E + 04	4.119E + 03	2.703E + 03
MCSA	**5.303E + 05**	**3.359E + 05**	1.220E + 04	1.061E + 04	**3.000E + 02**	**1.487E-02**
CSA	2.073E + 06	1.107E + 06	**8.918E + 03**	7.856E + 03	8.615E + 02	2.809E + 02
	F4		F5		F6	
	Avg	*Std*	*Avg*	*Std*	*Avg*	*Std*
VMCSA	4.923E + 02	**2.575E + 01**	5.201E + 02	2.179E-01	**6.187E + 02**	**1.929E + 00**
VCSA	5.676E + 02	4.332E + 01	5.201E + 02	2.187E-01	6.229E + 02	2.706E + 00
MCSA	**4.811E + 02**	3.224E + 01	**5.200E + 02**	7.535E-02	6.229E + 02	3.183E + 00
CSA	5.284E + 02	4.340E + 01	5.200E + 02	**5.245E-04**	6.302E + 02	3.208E + 00
	F7		F8		F9	
	Avg	*Std*	*Avg*	*Std*	*Avg*	*Std*
VMCSA	**7.000E + 02**	**1.142E-02**	**8.622E + 02**	1.934E + 01	**1.026E + 03**	3.376E + 01
VCSA	7.005E + 02	1.550E-01	8.992E + 02	2.049E + 01	1.050E + 03	2.549E + 01
MCSA	7.000E + 02	1.138E-02	9.136E + 02	2.256E + 01	1.026E + 03	**2.299E + 01**
CSA	7.000E + 02	2.509E-02	9.453E + 02	**1.884E + 01**	1.053E + 03	2.873E + 01
	F10		F11		F12	
	Avg	*Std*	*Avg*	*Std*	*Avg*	*Std*

(*continued on next page*)

Appendix A.2 (*continued*)

	F1		F2		F3	
	Avg	*Std*	*Avg*	*Std*	*Avg*	*Std*
VMCSA	**2.535E + 03**	5.881E + 02	**4.296E + 03**	6.612E + 02	**1.200E + 03**	**1.055E-01**
VCSA	2.771E + 03	6.401E + 02	4.449E + 03	6.428E + 02	1.200E + 03	8.728E-02
MCSA	4.047E + 03	6.387E + 02	4.937E + 03	7.188E + 02	1.201E + 03	2.842E-01
CSA	4.608E + 03	**4.678E + 02**	4.678E + 03	**6.067E + 02**	1.201E + 03	3.321E-01

	F13		F14		F15	
	Avg	*Std*	*Avg*	*Std*	*Avg*	*Std*
VMCSA	**1.300E + 03**	9.364E-02	**1.400E + 03**	**1.526E-01**	**1.515E + 03**	**6.000E + 00**
VCSA	1.300E + 03	**9.210E-02**	1.400E + 03	4.493E-02	1.520E + 03	6.746E + 00
MCSA	1.300E + 03	1.029E-01	1.400E + 03	1.973E-01	1.519E + 03	8.917E + 00
CSA	1.301E + 03	1.217E-01	1.400E + 03	5.260E-02	1.523E + 03	8.194E + 00

	F16		F17		F18	
	Avg	*Std*	*Avg*	*Std*	*Avg*	*Std*
VMCSA	**1.611E + 03**	6.551E-01	9.576E + 04	7.009E + 04	3.645E + 03	2.673E + 03
VCSA	1.611E + 03	**4.177E-01**	7.439E + 05	5.091E + 05	2.590E + 03	9.291E + 02
MCSA	1.612E + 03	5.231E-01	1.913E + 04	1.112E + 04	6.062E + 03	6.119E + 03
CSA	1.612E + 03	4.352E-01	**1.359E + 04**	**7.318E + 03**	**2.130E + 03**	**6.669E + 01**

	F19		F20		F21	
	Avg	*Std*	*Avg*	*Std*	*Avg*	*Std*
VMCSA	1.919E + 03	2.083E + 01	2.396E + 03	3.239E + 02	4.275E + 04	3.338E + 04
VCSA	1.927E + 03	2.436E + 01	4.159E + 03	1.793E + 03	1.498E + 05	1.120E + 05
MCSA	**1.917E + 03**	**9.849E + 00**	**2.310E + 03**	**8.896E + 01**	**1.242E + 04**	**5.835E + 03**
CSA	1.927E + 03	1.815E + 01	2.379E + 03	1.117E + 02	1.278E + 04	6.662E + 03

	F22		*F23*		F24	
	Avg	*Std*	*Avg*	*Std*	*Avg*	*Std*
VMCSA	**2.608E + 03**	**1.401E + 02**	**2.500E + 03**	3.045E-13	**2.600E + 03**	**1.924E-04**
VCSA	2.771E + 03	1.544E + 02	2.500E + 03	**2.388E-13**	2.600E + 03	3.406E-04
MCSA	2.742E + 03	2.149E + 02	2.615E + 03	2.925E-06	2.630E + 03	1.046E + 01
CSA	2.865E + 03	1.870E + 02	2.617E + 03	6.371E-01	2.615E + 03	1.206E + 01

	F25		F26		F27	
	Avg	*Std*	*Avg*	*Std*	*Avg*	*Std*
VMCSA	**2.700E + 03**	**8.444E-14**	**2.700E + 03**	**1.153E-01**	**2.900E + 03**	**1.689E-13**
VCSA	2.700E + 03	1.194E-13	2.704E + 03	1.817E + 01	2.900E + 03	3.870E-13
MCSA	2.715E + 03	3.678E + 00	2.700E + 03	1.255E-01	3.453E + 03	3.274E + 02
CSA	2.710E + 03	4.027E + 00	2.700E + 03	1.189E-01	3.165E + 03	1.870E + 02

	F28		F29		F30	
	Avg	*Std*	*Avg*	*Std*	*Avg*	*Std*
VMCSA	**3.000E + 03**	2.234E-13	**3.100E + 03**	**3.482E-13**	**3.200E + 03**	3.330E-06
VCSA	3.000E + 03	**2.068E-13**	3.100E + 03	4.547E-13	3.200E + 03	**8.174E-07**
MCSA	4.857E + 03	7.033E + 02	3.651E + 07	2.072E + 07	3.864E + 04	5.410E + 04
CSA	6.484E + 03	7.387E + 02	4.862E + 06	2.660E + 07	1.875E + 04	2.358E + 04

Appendix A.3
Results of different algorithms over average and standard deviation on CEC'21.

	F1		F2		F3	
	Avg	*Std*	*Avg*	*Std*	*Avg*	*Std*
VMCSA	**3.089E + 03**	**2.869E + 03**	4.325E + 03	7.294E + 02	**8.656E + 02**	**2.553E + 01**
SCA	1.337E + 10	2.080E + 09	8.132E + 03	2.655E + 02	1.145E + 03	4.804E + 01
m_SCA	5.846E + 09	2.849E + 09	4.853E + 03	8.457E + 02	9.951E + 02	6.278E + 01
MFO	1.428E + 10	7.402E + 09	4.935E + 03	5.751E + 02	1.194E + 03	1.612E + 02
GWO	1.879E + 09	1.536E + 09	**3.997E + 03**	**7.784E + 02**	8.721E + 02	4.109E + 01
SCADE	1.991E + 10	1.739E + 09	8.171E + 03	1.640E + 02	1.187E + 03	2.889E + 01
PSO	1.330E + 08	1.358E + 07	6.195E + 03	5.124E + 02	9.213E + 02	1.514E + 01
WOA	2.715E + 06	1.643E + 06	5.509E + 03	1.288E + 03	1.222E + 03	8.039E + 01
ACWOA	6.086E + 09	2.329E + 09	6.410E + 03	7.680E + 02	1.258E + 03	6.449E + 01
BMWOA	2.902E + 08	1.186E + 08	6.839E + 03	6.307E + 02	1.208E + 03	8.023E + 01

	F4		F5		F6	
	Avg	Std	Avg	Std	Avg	Std
VMCSA	**7.052E + 03**	**6.524E + 03**	**6.913E + 04**	**3.920E + 04**	2.505E + 03	3.175E + 02
SCA	2.535E + 07	1.039E + 07	5.885E + 06	2.254E + 06	3.696E + 03	1.868E + 02
m_SCA	3.251E + 06	3.964E + 06	1.434E + 06	1.252E + 06	2.639E + 03	1.235E + 02
MFO	9.878E + 06	2.362E + 07	2.970E + 06	4.394E + 06	3.065E + 03	4.035E + 02
GWO	1.806E + 06	2.941E + 06	1.731E + 06	1.866E + 06	**2.444E + 03**	**2.444E + 02**
SCADE	2.261E + 07	1.099E + 07	1.370E + 07	8.455E + 06	3.781E + 03	2.203E + 02
PSO	1.469E + 06	4.950E + 05	3.718E + 05	1.980E + 05	2.943E + 03	2.684E + 02
WOA	3.157E + 06	2.436E + 06	3.435E + 06	2.709E + 06	3.482E + 03	5.405E + 02
ACWOA	5.653E + 06	2.440E + 06	1.205E + 07	8.513E + 06	3.958E + 03	2.408E + 02
BMWOA	4.707E + 05	4.194E + 05	6.252E + 06	2.459E + 06	3.270E + 03	3.641E + 02

	F7		F8		F9	
	Avg	*Std*	*Avg*	*Std*	*Avg*	*Std*
VMCSA	**5.452E + 04**	**2.713E + 04**	**2.300E + 03**	**7.889E-01**	2.930E + 03	2.387E + 01
SCA	1.279E + 06	5.823E + 05	7.840E + 03	2.554E + 03	3.165E + 03	2.780E + 01
m_SCA	3.348E + 05	3.224E + 05	5.698E + 03	1.389E + 03	2.961E + 03	3.958E + 01
MFO	8.729E + 05	1.368E + 06	6.281E + 03	1.691E + 03	2.989E + 03	2.307E + 01
GWO	3.988E + 05	4.166E + 05	4.064E + 03	1.372E + 03	**2.929E + 03**	**5.437E + 01**
SCADE	2.575E + 06	7.289E + 05	4.613E + 03	3.494E + 02	3.186E + 03	2.962E + 01
PSO	8.070E + 04	4.490E + 04	5.832E + 03	3.015E + 03	3.180E + 03	8.128E + 01
WOA	1.240E + 06	1.326E + 06	7.289E + 03	1.342E + 03	3.143E + 03	6.300E + 01
ACWOA	5.268E + 06	4.432E + 06	5.277E + 03	2.194E + 03	3.193E + 03	1.103E + 02
BMWOA	8.733E + 05	7.260E + 05	4.522E + 03	3.133E + 03	3.101E + 03	9.266E + 01

	F10	
	Avg	*Std*
VMCSA	2.908E+03	1.940E+01
SCA	3.210E+03	1.161E+02
m_SCA	3.021E+03	3.878E+01
MFO	3.559E+03	7.542E+02
GWO	2.980E+03	4.438E+01
SCADE	3.470E+03	1.299E+02
PSO	**2.900E+03**	**2.249E+01**
WOA	2.954E+03	4.212E+01
ACWOA	3.211E+03	1.469E+02
BMWOA	3.023E+03	3.239E+01

Appendix A.4

Comparison different algorithms according to the PSNR average and standard deviation.

Image	K		VMCSA	CSA	DE	HHO	PSO	CS	BLPSO	IWOA	IGWO	CGPSO
X-ray image 1	8	*Avg*	**2.425E + 01**	2.382E + 01	2.308E + 01	2.292E + 01	2.385E + 01	2.306E + 01	2.247E + 01	2.195E + 01	2.253E + 01	2.409E + 01
		Std	**5.566E-01**	1.005E + 00	1.080E + 00	2.031E + 00	8.528E-01	1.275E + 00	1.027E + 00	2.237E + 00	1.536E + 00	8.278E-01
	10	*Avg*	**2.582E + 01**	2.461E + 01	2.494E + 01	2.392E + 01	2.532E + 01	2.430E + 01	2.395E + 01	2.322E + 01	2.444E + 01	2.572E + 01
		Std	**7.343E-01**	1.574E + 00	8.489E-01	2.114E + 00	1.084E + 00	1.454E + 00	1.076E + 00	2.454E + 00	1.545E + 00	8.425E-01
	15	*Avg*	**2.876E + 01**	2.840E + 01	2.675E + 01	2.635E + 01	2.795E + 01	2.728E + 01	2.573E + 01	2.651E + 01	2.625E + 01	2.830E + 01
		Std	**8.402E-01**	9.039E-01	1.117E + 00	2.952E + 00	1.018E + 00	1.080E + 00	1.456E + 00	1.787E + 00	1.522E + 00	1.056E + 00
	18	*Avg*	**3.058E + 01**	3.021E + 01	2.837E + 01	2.789E + 01	2.911E + 01	2.854E + 01	2.694E + 01	2.681E + 01	2.689E + 01	2.910E + 01
		Std	**7.595E-01**	8.387E-01	9.902E-01	1.839E + 00	1.300E + 00	1.142E + 00	1.454E + 00	2.844E + 00	2.078E + 00	9.825E-01
	20	*Avg*	**3.134E + 01**	3.057E + 01	2.939E + 01	2.877E + 01	2.924E + 01	2.948E + 01	2.767E + 01	2.756E + 01	2.774E + 01	2.933E + 01
		Std	**6.490E-01**	8.770E-01	1.075E + 00	1.853E + 00	1.032E + 00	1.252E + 00	1.553E + 00	1.626E + 00	2.310E + 00	1.588E + 00
X-ray image 2	8	*Avg*	2.367E + 01	2.361E + 01	2.274E + 01	2.262E + 01	**2.374E + 01**	2.261E + 01	2.187E + 01	2.188E + 01	2.168E + 01	2.355E + 01
		Std	**6.112E-01**	1.260E + 00	1.247E + 00	2.139E + 00	6.830E-01	1.375E + 00	1.587E + 00	1.963E + 00	1.241E + 00	1.344E + 00
	10	*Avg*	**2.547E + 01**	2.520E + 01	2.410E + 01	2.361E + 01	2.475E + 01	2.452E + 01	2.306E + 01	2.328E + 01	2.329E + 01	2.531E + 01
		Std	**4.253E-01**	8.558E-01	1.246E + 00	2.494E + 00	6.666E-01	1.159E + 00	1.281E + 00	1.568E + 00	1.458E + 00	7.394E-01
	15	*Avg*	**2.878E + 01**	2.852E + 01	2.688E + 01	2.690E + 01	2.715E + 01	2.715E + 01	2.512E + 01	2.619E + 01	2.521E + 01	2.802E + 01
		Std	**5.017E-01**	7.151E-01	8.598E-01	1.601E + 00	1.166E + 00	1.436E + 00	1.575E + 00	1.419E + 00	1.634E + 00	7.308E-01
	18	*Avg*	**3.036E + 01**	2.983E + 01	2.829E + 01	2.731E + 01	2.890E + 01	2.797E + 01	2.648E + 01	2.678E + 01	2.652E + 01	2.927E + 01
		Std	**6.593E-01**	9.576E-01	1.112E + 00	1.802E + 00	8.847E-01	1.198E + 00	1.261E + 00	1.970E + 00	1.587E + 00	7.411E-01
	20	*Avg*	**3.086E + 01**	3.079E + 01	2.893E + 01	2.771E + 01	2.953E + 01	2.865E + 01	2.760E + 01	2.784E + 01	2.781E + 01	2.975E + 01
		Std	**5.206E-01**	7.164E-01	8.178E-01	3.054E + 00	8.449E-01	1.423E + 00	2.042E + 00	1.941E + 00	1.614E + 00	1.131E + 00
X-ray image 3	8	*Avg*	**2.352E + 01**	2.314E + 01	2.232E + 01	2.184E + 01	2.351E + 01	2.182E + 01	2.193E + 01	2.117E + 01	2.181E + 01	2.347E + 01
		Std	**5.333E-01**	9.914E-01	1.120E + 00	2.701E + 00	6.760E-01	1.437E + 00	1.430E + 00	1.697E + 00	1.242E + 00	7.871E-01
	10	*Avg*	**2.567E + 01**	2.479E + 01	2.446E + 01	2.357E + 01	2.497E + 01	2.409E + 01	2.292E + 01	2.288E + 01	2.305E + 01	2.524E + 01
		Std	**4.060E-01**	1.296E + 00	6.818E-01	1.366E + 00	9.979E-01	1.357E + 00	1.048E + 00	2.260E + 00	1.966E + 00	7.270E-01
	15	*Avg*	**2.861E + 01**	2.797E + 01	2.691E + 01	2.599E + 01	2.752E + 01	2.572E + 01	2.492E + 01	2.591E + 01	2.523E + 01	2.784E + 01
		Std	**4.657E-01**	8.212E-01	8.317E-01	2.467E + 00	5.765E-01	2.253E + 00	1.342E + 00	1.706E + 00	2.120E + 00	1.050E + 00
	18	*Avg*	**3.017E + 01**	2.961E + 01	2.836E + 01	2.751E + 01	2.872E + 01	2.776E + 01	2.622E + 01	2.597E + 01	2.671E + 01	2.902E + 01
		Std	8.346E-01	9.024E-01	**7.682E-01**	1.728E + 00	1.277E + 00	1.140E + 00	1.606E + 00	2.407E + 00	1.340E + 00	9.979E-01
	20	*Avg*	**3.077E + 01**	3.056E + 01	2.922E + 01	2.759E + 01	2.955E + 01	2.829E + 01	2.779E + 01	2.714E + 01	2.712E + 01	2.958E + 01
		Std	9.298E-01	9.041E-01	1.023E + 00	2.081E + 00	9.520E-01	1.781E + 00	1.442E + 00	1.824E + 00	1.561E + 00	**7.372E-01**
X-ray image 4	8	*Avg*	**2.415E + 01**	2.371E + 01	2.268E + 01	2.155E + 01	2.326E + 01	2.171E + 01	2.177E + 01	2.147E + 01	2.126E + 01	2.361E + 01
		Std	**4.657E-01**	7.971E-01	7.834E-01	2.070E + 00	1.043E + 00	1.333E + 00	8.732E-01	2.255E + 00	1.479E + 00	1.172E + 00
	10	*Avg*	**2.565E + 01**	2.531E + 01	2.433E + 01	2.395E + 01	2.461E + 01	2.319E + 01	2.291E + 01	2.305E + 01	2.300E + 01	2.533E + 01
		Std	**4.280E-01**	5.405E-01	9.676E-01	1.454E + 00	1.379E + 00	1.389E + 00	9.670E-01	1.581E + 00	1.511E + 00	6.587E-01
	15	*Avg*	**2.902E + 01**	2.818E + 01	2.728E + 01	2.656E + 01	2.758E + 01	2.652E + 01	2.522E + 01	2.532E + 01	2.537E + 01	2.805E + 01

(*continued on next page*)

Appendix A.4 (*continued*)

Image	K		VMCSA	CSA	DE	HHO	PSO	CS	BLPSO	IWOA	IGWO	CGPSO
		Std	**3.488E-01**	7.959E-01	7.119E-01	1.524E + 00	1.215E + 00	1.227E + 00	1.091E + 00	1.965E + 00	1.684E + 00	1.175E + 00
	18	*Avg*	**3.039E + 01**	2.986E + 01	2.845E + 01	2.666E + 01	2.849E + 01	2.812E + 01	2.654E + 01	2.647E + 01	2.594E + 01	2.933E + 01
		Std	**3.456E-01**	5.945E-01	6.556E-01	2.076E + 00	1.020E + 00	8.908E-01	1.393E + 00	1.276E + 00	1.284E + 00	7.588E-01
	20	*Avg*	**3.135E + 01**	3.068E + 01	2.902E + 01	2.729E + 01	2.882E + 01	2.870E + 01	2.719E + 01	2.713E + 01	2.757E + 01	2.980E + 01
		Std	**5.007E-01**	5.754E-01	1.027E + 00	2.945E + 00	1.302E + 00	9.420E-01	1.810E + 00	1.739E + 00	1.266E + 00	1.054E + 00
X-ray image 5	8	*Avg*	2.359E + 01	**2.361E + 01**	2.255E + 01	2.107E + 01	2.357E + 01	2.214E + 01	2.176E + 01	2.149E + 01	2.196E + 01	2.345E + 01
		Std	8.900E-01	6.568E-01	1.025E + 00	2.116E + 00	**5.190E-01**	1.844E + 00	1.343E + 00	1.868E + 00	2.252E + 00	1.205E + 00
	10	*Avg*	**2.535E + 01**	2.513E + 01	2.424E + 01	2.363E + 01	2.498E + 01	2.454E + 01	2.321E + 01	2.310E + 01	2.343E + 01	2.522E + 01
		Std	**4.794E-01**	1.094E + 00	1.028E + 00	2.387E + 00	8.187E-01	8.856E-01	1.787E + 00	2.025E + 00	2.104E + 00	4.927E-01
	15	*Avg*	**2.862E + 01**	2.808E + 01	2.699E + 01	2.559E + 01	2.781E + 01	2.659E + 01	2.578E + 01	2.638E + 01	2.607E + 01	2.756E + 01
		Std	**4.500E-01**	9.295E-01	1.047E + 00	2.270E + 00	8.002E-01	1.654E + 00	1.166E + 00	1.389E + 00	1.402E + 00	1.043E + 00
	18	*Avg*	**3.018E + 01**	2.995E + 01	2.837E + 01	2.679E + 01	2.909E + 01	2.801E + 01	2.731E + 01	2.724E + 01	2.641E + 01	2.918E + 01
		Std	**5.366E-01**	5.517E-01	1.210E + 00	2.119E + 00	8.524E-01	1.118E + 00	9.554E-01	1.616E + 00	2.005E + 00	1.123E + 00
	20	*Avg*	**3.089E + 01**	3.082E + 01	2.933E + 01	2.794E + 01	2.961E + 01	2.871E + 01	2.712E + 01	2.828E + 01	2.807E + 01	3.024E + 01
		Std	**4.525E-01**	7.524E-01	7.808E-01	2.764E + 00	1.233E + 00	1.437E + 00	1.808E + 00	1.906E + 00	1.181E + 00	1.118E + 00
X-ray image 6	8	*Avg*	2.359E + 01	2.320E + 01	2.304E + 01	2.108E + 01	**2.371E + 01**	2.210E + 01	2.204E + 01	2.124E + 01	2.109E + 01	2.337E + 01
		Std	8.976E-01	1.604E + 00	**7.227E-01**	2.807E + 00	9.764E-01	1.318E + 00	1.185E + 00	2.297E + 00	1.778E + 00	1.125E + 00
	10	*Avg*	**2.544E + 01**	2.518E + 01	2.484E + 01	2.287E + 01	2.457E + 01	2.404E + 01	2.339E + 01	2.304E + 01	2.278E + 01	2.456E + 01
		Std	**5.859E-01**	8.455E-01	7.798E-01	1.663E + 00	1.115E + 00	1.242E + 00	9.274E-01	1.559E + 00	1.358E + 00	1.135E + 00
	15	*Avg*	**2.866E + 01**	2.832E + 01	2.720E + 01	2.667E + 01	2.779E + 01	2.648E + 01	2.527E + 01	2.570E + 01	2.533E + 01	2.815E + 01
		Std	8.441E-01	7.615E-01	**7.354E-01**	1.728E + 00	7.427E-01	1.831E + 00	1.497E + 00	1.644E + 00	2.502E + 00	1.153E + 00
	18	*Avg*	**3.043E + 01**	3.021E + 01	2.848E + 01	2.743E + 01	2.887E + 01	2.777E + 01	2.696E + 01	2.742E + 01	2.705E + 01	2.944E + 01
		Std	5.225E-01	**3.238E-01**	1.121E + 00	1.989E + 00	9.963E-01	1.184E + 00	1.281E + 00	1.508E + 00	1.500E + 00	8.462E-01
	20	*Avg*	**3.139E + 01**	3.113E + 01	2.942E + 01	2.813E + 01	2.978E + 01	2.938E + 01	2.735E + 01	2.715E + 01	2.659E + 01	3.024E + 01
		Std	5.145E-01	**4.882E-01**	9.924E-01	1.794E + 00	9.166E-01	1.127E + 00	1.248E + 00	1.708E + 00	1.971E + 00	8.137E-01

Appendix A.5

Comparison different algorithms according to the SSIM average and standard deviation.

Image	K		VMCSA	CSA	DE	HHO	PSO	CS	BLPSO	IWOA	IGWO	CGPSO
X-ray image 1	8	*Avg*	7.261E-01	7.145E-01	6.984E-01	6.947E-01	7.207E-01	7.012E-01	6.892E-01	6.814E-01	6.900E-01	**7.282E-01**
		Std	**1.830E-02**	3.525E-02	3.141E-02	7.489E-02	2.786E-02	3.845E-02	3.144E-02	6.819E-02	5.925E-02	3.151E-02
	10	*Avg*	**7.774E-01**	7.432E-01	7.587E-01	7.383E-01	7.645E-01	7.386E-01	7.393E-01	7.098E-01	7.415E-01	7.746E-01
		Std	**1.988E-02**	4.690E-02	2.596E-02	6.935E-02	3.101E-02	4.473E-02	3.531E-02	8.515E-02	4.372E-02	2.656E-02
	15	*Avg*	**8.528E-01**	8.465E-01	8.139E-01	8.155E-01	8.383E-01	8.231E-01	7.884E-01	8.060E-01	7.992E-01	8.470E-01
		Std	**1.804E-02**	2.026E-02	2.067E-02	5.341E-02	2.282E-02	2.598E-02	3.548E-02	3.561E-02	3.642E-02	2.413E-02
	18	*Avg*	**8.907E-01**	8.832E-01	8.448E-01	8.426E-01	8.627E-01	8.509E-01	8.174E-01	8.141E-01	8.153E-01	8.609E-01
		Std	**1.392E-02**	1.565E-02	1.956E-02	3.933E-02	2.392E-02	2.336E-02	3.194E-02	5.826E-02	4.524E-02	2.092E-02
	20	*Avg*	**9.047E-01**	8.909E-01	8.680E-01	8.594E-01	8.637E-01	8.694E-01	8.290E-01	8.387E-01	8.380E-01	8.674E-01
		Std	**1.190E-02**	1.482E-02	2.120E-02	3.446E-02	2.030E-02	2.467E-02	3.281E-02	3.142E-02	4.828E-02	2.797E-02
X-ray image 2	8	*Avg*	7.781E-01	7.791E-01	7.640E-01	7.735E-01	7.770E-01	**7.837E-01**	7.710E-01	7.543E-01	7.725E-01	7.695E-01
		Std	1.739E-02	1.536E-02	**1.297E-02**	3.455E-02	1.214E-02	1.680E-02	2.528E-02	4.597E-02	3.109E-02	4.690E-02
	10	*Avg*	**8.058E-01**	8.054E-01	7.963E-01	7.952E-01	8.004E-01	8.048E-01	7.816E-01	7.883E-01	7.817E-01	8.024E-01
		Std	**9.870E-03**	1.732E-02	1.720E-02	3.920E-02	1.805E-02	1.885E-02	2.033E-02	2.380E-02	4.028E-02	1.232E-02
	15	*Avg*	**8.588E-01**	8.539E-01	8.358E-01	8.440E-01	8.427E-01	8.440E-01	8.137E-01	8.282E-01	8.214E-01	8.490E-01
		Std	**7.907E-03**	1.029E-02	1.040E-02	2.636E-02	1.498E-02	1.741E-02	2.265E-02	2.439E-02	2.186E-02	1.229E-02
	18	*Avg*	**8.836E-01**	8.770E-01	8.561E-01	8.555E-01	8.648E-01	8.577E-01	8.360E-01	8.504E-01	8.461E-01	8.728E-01
		Std	**7.493E-03**	1.172E-02	1.267E-02	2.516E-02	1.271E-02	1.212E-02	1.857E-02	2.297E-02	2.797E-02	1.409E-02
	20	*Avg*	**8.922E-01**	8.906E-01	8.685E-01	8.575E-01	8.744E-01	8.674E-01	8.534E-01	8.573E-01	8.554E-01	8.789E-01
		Std	**7.182E-03**	8.112E-03	1.096E-02	3.961E-02	1.463E-02	1.418E-02	1.924E-02	1.733E-02	2.581E-02	1.716E-02
X-ray image 3	8	*Avg*	7.638E-01	7.592E-01	7.529E-01	7.621E-01	7.558E-01	**7.643E-01**	7.544E-01	7.400E-01	7.584E-01	7.585E-01
		Std	1.678E-02	**1.540E-02**	2.445E-02	7.278E-02	1.976E-02	2.814E-02	1.983E-02	4.404E-02	2.276E-02	2.508E-02
	10	*Avg*	**7.998E-01**	7.916E-01	7.813E-01	7.766E-01	7.862E-01	7.850E-01	7.596E-01	7.726E-01	7.930E-01	7.928E-01
		Std	**1.070E-02**	2.417E-02	1.565E-02	3.965E-02	1.730E-02	2.958E-02	2.163E-02	4.027E-02	2.395E-02	2.075E-02
	15	*Avg*	**8.511E-01**	8.480E-01	8.250E-01	8.289E-01	8.354E-01	8.230E-01	8.022E-01	8.187E-01	8.143E-01	8.422E-01
		Std	**1.065E-02**	1.180E-02	1.405E-02	3.495E-02	1.157E-02	3.169E-02	2.093E-02	2.633E-02	2.811E-02	2.077E-02
	18	*Avg*	**8.783E-01**	8.761E-01	8.520E-01	8.514E-01	8.625E-01	8.492E-01	8.255E-01	8.335E-01	8.411E-01	8.665E-01
		Std	**9.411E-03**	1.210E-02	1.041E-02	3.286E-02	1.829E-02	1.791E-02	2.392E-02	2.300E-02	2.292E-02	1.472E-02
	20	*Avg*	**8.910E-01**	8.873E-01	8.688E-01	8.542E-01	8.714E-01	8.588E-01	8.488E-01	8.448E-01	8.442E-01	8.772E-01
		Std	1.093E-02	1.086E-02	1.439E-02	2.393E-02	1.439E-02	2.127E-02	1.645E-02	2.998E-02	2.053E-02	**1.042E-02**
X-ray image 4	8	*Avg*	7.663E-01	**7.679E-01**	7.484E-01	7.396E-01	7.638E-01	7.440E-01	7.353E-01	7.456E-01	7.154E-01	7.673E-01
		Std	**1.124E-02**	2.086E-02	1.706E-02	3.378E-02	1.840E-02	3.497E-02	2.092E-02	2.912E-02	3.191E-02	1.877E-02
	10	*Avg*	**8.004E-01**	7.988E-01	7.803E-01	7.864E-01	7.854E-01	7.768E-01	7.686E-01	7.761E-01	7.585E-01	7.986E-01
		Std	**8.071E-03**	1.281E-02	1.582E-02	2.495E-02	2.205E-02	3.358E-02	2.639E-02	2.193E-02	1.635E-02	1.593E-02
	15	*Avg*	**8.622E-01**	8.554E-01	8.375E-01	8.330E-01	8.432E-01	8.298E-01	8.111E-01	8.222E-01	8.181E-01	8.510E-01
		Std	**4.397E-03**	1.139E-02	1.255E-02	2.161E-02	1.980E-02	1.811E-02	2.116E-02	2.389E-02	2.547E-02	1.818E-02
	18	*Avg*	**8.875E-01**	8.824E-01	8.555E-01	8.455E-01	8.649E-01	8.610E-01	8.309E-01	8.409E-01	8.281E-01	8.747E-01
		Std	**4.912E-03**	1.054E-02	9.228E-03	2.958E-02	1.518E-02	1.596E-02	2.385E-02	2.190E-02	1.737E-02	1.102E-02
	20	*Avg*	**9.021E-01**	8.939E-01	8.729E-01	8.568E-01	8.713E-01	8.715E-01	8.448E-01	8.542E-01	8.551E-01	8.842E-01
		Std	**6.745E-03**	7.068E-03	1.230E-02	3.619E-02	1.559E-02	1.183E-02	2.299E-02	2.431E-02	2.183E-02	1.121E-02
X-ray image 5	8	*Avg*	**7.548E-01**	7.522E-01	7.345E-01	7.300E-01	7.482E-01	7.350E-01	7.257E-01	7.231E-01	7.247E-01	7.421E-01
		Std	2.237E-02	2.080E-02	**1.705E-02**	6.171E-02	1.783E-02	5.237E-02	3.130E-02	5.898E-02	6.083E-02	3.389E-02
	10	*Avg*	**7.876E-01**	7.831E-01	7.634E-01	7.667E-01	7.728E-01	7.697E-01	7.504E-01	7.587E-01	7.614E-01	7.841E-01
		Std	1.899E-02	2.380E-02	1.733E-02	5.324E-02	1.931E-02	1.900E-02	4.622E-02	4.569E-02	3.943E-02	**1.557E-02**
	15	*Avg*	**8.497E-01**	8.444E-01	8.227E-01	8.030E-01	8.457E-01	8.216E-01	8.056E-01	8.244E-01	8.221E-01	8.386E-01
		Std	**9.956E-03**	1.592E-02	2.226E-02	4.490E-02	1.578E-02	2.525E-02	2.042E-02	2.395E-02	2.686E-02	1.709E-02
	18	*Avg*	**8.782E-01**	8.754E-01	8.535E-01	8.392E-01	8.626E-01	8.502E-01	8.348E-01	8.368E-01	8.201E-01	8.674E-01
		Std	**9.071E-03**	9.591E-03	1.592E-02	3.460E-02	1.525E-02	1.993E-02	1.737E-02	3.084E-02	3.669E-02	2.007E-02
	20	*Avg*	8.903E-01	**8.907E-01**	8.698E-01	8.499E-01	8.734E-01	8.602E-01	8.341E-01	8.521E-01	8.490E-01	8.808E-01
		Std	**5.479E-03**	1.195E-02	1.155E-02	4.065E-02	1.987E-02	2.169E-02	2.961E-02	2.994E-02	1.798E-02	1.851E-02
X-ray image 6	8	*Avg*	7.772E-01	7.691E-01	7.775E-01	7.611E-01	**7.821E-01**	7.615E-01	7.575E-01	7.513E-01	7.676E-01	7.735E-01
		Std	2.790E-02	4.637E-02	1.325E-02	5.495E-02	**9.062E-03**	2.477E-02	2.461E-02	4.090E-02	5.936E-02	3.943E-02
	10	*Avg*	8.102E-01	**8.112E-01**	7.989E-01	8.021E-01	8.088E-01	7.930E-01	7.784E-01	7.791E-01	7.783E-01	8.020E-01
		Std	**1.361E-02**	1.486E-02	1.514E-02	3.181E-02	2.121E-02	3.017E-02	2.135E-02	3.573E-02	3.830E-02	2.949E-02
	15	*Avg*	**8.691E-01**	8.590E-01	8.433E-01	8.527E-01	8.582E-01	8.430E-01	8.252E-01	8.267E-01	8.271E-01	8.642E-01
		Std	**6.797E-03**	1.148E-02	1.174E-02	2.846E-02	1.426E-02	2.789E-02	1.731E-02	2.798E-02	2.629E-02	1.523E-02
	18	*Avg*	**8.934E-01**	8.886E-01	8.667E-01	8.619E-01	8.734E-01	8.639E-01	8.473E-01	8.590E-01	8.545E-01	8.811E-01
		Std	**5.550E-03**	5.829E-03	9.396E-03	2.797E-02	1.435E-02	1.718E-02	1.944E-02	2.076E-02	1.769E-02	1.275E-02
	20	*Avg*	**9.051E-01**	9.015E-01	8.786E-01	8.769E-01	8.870E-01	8.829E-01	8.569E-01	8.587E-01	8.612E-01	8.930E-01
		Std	6.606E-03	**6.417E-03**	1.237E-02	1.931E-02	1.314E-02	1.382E-02	1.623E-02	2.389E-02	1.655E-02	7.628E-03

Appendix A.6

Comparison different algorithms according to the FSIM average and standard deviation.

Image	K		VMCSA	CSA	DE	HHO	PSO	CS	BLPSO	IWOA	IGWO	CGPSO
X-ray image 1	8	*Avg*	**8.850E-01**	8.766E-01	8.500E-01	8.480E-01	8.720E-01	8.477E-01	8.252E-01	8.219E-01	8.357E-01	8.788E-01
		Std	**1.518E-02**	2.344E-02	3.101E-02	5.114E-02	2.233E-02	3.353E-02	3.024E-02	5.489E-02	3.791E-02	2.172E-02
	10	*Avg*	**9.206E-01**	8.954E-01	8.983E-01	8.709E-01	9.064E-01	8.824E-01	8.713E-01	8.573E-01	8.822E-01	9.166E-01
		Std	**1.529E-02**	3.062E-02	1.950E-02	4.914E-02	2.498E-02	3.226E-02	2.703E-02	5.681E-02	3.849E-02	1.843E-02
	15	*Avg*	**9.649E-01**	9.554E-01	9.238E-01	9.106E-01	9.451E-01	9.347E-01	8.997E-01	9.150E-01	9.069E-01	9.490E-01
		Std	**8.567E-03**	1.068E-02	2.342E-02	5.522E-02	1.542E-02	1.724E-02	2.775E-02	3.334E-02	2.712E-02	1.415E-02
	18	*Avg*	**9.790E-01**	9.716E-01	9.462E-01	9.364E-01	9.540E-01	9.493E-01	9.160E-01	9.162E-01	9.166E-01	9.576E-01
		Std	**5.645E-03**	8.521E-03	1.505E-02	2.587E-02	2.086E-02	1.714E-02	2.740E-02	4.793E-02	3.346E-02	1.049E-02
	20	*Avg*	**9.829E-01**	9.731E-01	9.554E-01	9.446E-01	9.597E-01	9.576E-01	9.266E-01	9.310E-01	9.305E-01	9.551E-01
		Std	**3.834E-03**	8.687E-03	1.697E-02	2.521E-02	1.015E-02	1.571E-02	2.702E-02	2.504E-02	3.285E-02	1.763E-02
X-ray image 2	8	*Avg*	8.141E-01	**8.195E-01**	7.963E-01	8.086E-01	8.155E-01	8.084E-01	7.910E-01	7.960E-01	7.941E-01	8.142E-01
		Std	1.254E-02	2.050E-02	2.326E-02	3.434E-02	**1.143E-02**	1.996E-02	2.479E-02	2.746E-02	1.769E-02	2.518E-02
	10	*Avg*	**8.533E-01**	8.517E-01	8.318E-01	8.301E-01	8.409E-01	8.420E-01	8.106E-01	8.226E-01	8.205E-01	8.497E-01
		Std	**1.013E-02**	1.726E-02	2.299E-02	4.070E-02	1.786E-02	2.662E-02	2.363E-02	2.737E-02	2.141E-02	1.533E-02
	15	*Avg*	**9.174E-01**	9.112E-01	8.846E-01	8.876E-01	8.909E-01	8.875E-01	8.506E-01	8.672E-01	8.546E-01	9.007E-01
		Std	**9.953E-03**	1.275E-02	1.246E-02	2.788E-02	1.856E-02	2.108E-02	2.797E-02	3.071E-02	2.684E-02	1.263E-02
	18	*Avg*	**9.412E-01**	9.302E-01	9.038E-01	8.920E-01	9.147E-01	8.995E-01	8.736E-01	8.827E-01	8.803E-01	9.201E-01
		Std	**9.670E-03**	1.523E-02	1.951E-02	2.526E-02	1.523E-02	1.747E-02	2.428E-02	3.096E-02	2.420E-02	1.147E-02
	20	*Avg*	**9.464E-01**	9.435E-01	9.138E-01	9.023E-01	9.247E-01	9.079E-01	8.940E-01	8.983E-01	8.903E-01	9.232E-01
		Std	**7.703E-03**	1.048E-02	1.345E-02	3.631E-02	1.157E-02	2.237E-02	2.550E-02	2.722E-02	3.317E-02	1.857E-02
X-ray image 3	8	*Avg*	8.125E-01	8.029E-01	7.897E-01	8.054E-01	**8.129E-01**	7.962E-01	7.881E-01	7.812E-01	7.827E-01	8.097E-01
		Std	**1.557E-02**	2.210E-02	2.146E-02	4.542E-02	1.985E-02	2.613E-02	2.919E-02	4.102E-02	2.674E-02	1.922E-02
	10	*Avg*	**8.660E-01**	8.500E-01	8.329E-01	8.312E-01	8.468E-01	8.383E-01	8.030E-01	8.154E-01	8.214E-01	8.533E-01
		Std	**7.884E-03**	2.061E-02	1.600E-02	3.023E-02	2.286E-02	3.063E-02	2.386E-02	4.164E-02	3.127E-02	1.834E-02
	15	*Avg*	**9.211E-01**	9.082E-01	8.861E-01	8.695E-01	9.002E-01	8.674E-01	8.422E-01	8.670E-01	8.495E-01	9.055E-01
		Std	**8.640E-03**	1.779E-02	1.501E-02	4.867E-02	9.745E-03	4.113E-02	2.656E-02	3.488E-02	4.133E-02	1.712E-02
	18	*Avg*	**9.429E-01**	9.322E-01	9.077E-01	9.004E-01	9.151E-01	8.986E-01	8.702E-01	8.703E-01	8.800E-01	9.234E-01
		Std	1.413E-02	**1.328E-02**	1.555E-02	2.444E-02	2.515E-02	2.190E-02	2.911E-02	3.201E-02	2.726E-02	1.370E-02
	20	*Avg*	**9.488E-01**	9.434E-01	9.225E-01	8.961E-01	9.277E-01	9.071E-01	8.949E-01	8.863E-01	8.871E-01	9.281E-01
		Std	1.451E-02	1.363E-02	1.880E-02	2.971E-02	1.714E-02	2.459E-02	2.592E-02	3.394E-02	2.856E-02	**1.237E-02**
X-ray image 4	8	*Avg*	**8.347E-01**	8.289E-01	8.032E-01	7.945E-01	8.226E-01	7.969E-01	7.851E-01	7.945E-01	7.785E-01	8.308E-01
		Std	**7.571E-03**	1.727E-02	2.019E-02	4.511E-02	1.763E-02	2.795E-02	2.658E-02	3.843E-02	3.528E-02	2.702E-02
	10	*Avg*	**8.718E-01**	8.679E-01	8.400E-01	8.467E-01	8.569E-01	8.293E-01	8.164E-01	8.197E-01	8.134E-01	8.657E-01
		Std	**8.619E-03**	1.509E-02	2.472E-02	3.224E-02	1.986E-02	2.588E-02	3.231E-02	3.408E-02	3.298E-02	1.653E-02
	15	*Avg*	**9.365E-01**	9.202E-01	9.007E-01	8.908E-01	9.074E-01	8.878E-01	8.586E-01	8.646E-01	8.737E-01	9.163E-01
		Std	**6.325E-03**	1.620E-02	1.467E-02	3.037E-02	2.692E-02	2.715E-02	2.703E-02	3.661E-02	2.378E-02	2.515E-02
	18	*Avg*	**9.541E-01**	9.436E-01	9.158E-01	8.980E-01	9.225E-01	9.142E-01	8.837E-01	8.883E-01	8.789E-01	9.324E-01
		Std	**5.379E-03**	1.018E-02	1.234E-02	2.815E-02	1.733E-02	1.635E-02	2.716E-02	2.566E-02	2.594E-02	1.538E-02
	20	*Avg*	**9.635E-01**	9.515E-01	9.264E-01	9.052E-01	9.258E-01	9.254E-01	8.919E-01	8.993E-01	9.069E-01	9.378E-01
		Std	**6.323E-03**	9.117E-03	2.005E-02	4.219E-02	2.153E-02	1.660E-02	3.480E-02	2.549E-02	2.048E-02	1.304E-02
X-ray image 5	8	*Avg*	**8.625E-01**	8.595E-01	8.361E-01	8.171E-01	8.541E-01	8.323E-01	8.211E-01	8.143E-01	8.241E-01	8.569E-01
		Std	**1.417E-02**	1.911E-02	2.066E-02	4.061E-02	1.603E-02	3.801E-02	3.175E-02	4.416E-02	5.242E-02	1.714E-02
	10	*Avg*	**8.978E-01**	8.877E-01	8.649E-01	8.646E-01	8.852E-01	8.747E-01	8.464E-01	8.535E-01	8.557E-01	8.928E-01
		Std	**1.367E-02**	2.759E-02	2.496E-02	4.782E-02	1.770E-02	2.164E-02	3.622E-02	3.073E-02	4.001E-02	1.397E-02
	15	*Avg*	**9.517E-01**	9.392E-01	9.167E-01	8.931E-01	9.370E-01	9.093E-01	8.943E-01	9.045E-01	9.009E-01	9.300E-01
		Std	**6.069E-03**	1.589E-02	2.266E-02	3.976E-02	1.035E-02	3.110E-02	2.551E-02	2.554E-02	2.666E-02	1.607E-02
	18	*Avg*	**9.671E-01**	9.607E-01	9.386E-01	9.160E-01	9.479E-01	9.336E-01	9.212E-01	9.169E-01	9.000E-01	9.466E-01
		Std	**5.619E-03**	6.567E-03	2.080E-02	2.958E-02	1.208E-02	1.888E-02	1.721E-02	2.900E-02	3.464E-02	1.802E-02
	20	*Avg*	**9.723E-01**	9.680E-01	9.508E-01	9.292E-01	9.488E-01	9.386E-01	9.130E-01	9.311E-01	9.290E-01	9.563E-01
		Std	**4.413E-03**	7.004E-03	1.065E-02	3.089E-02	1.680E-02	1.979E-02	2.647E-02	2.849E-02	1.833E-02	1.520E-02
X-ray image 6	8	*Avg*	8.463E-01	8.404E-01	8.334E-01	8.132E-01	**8.476E-01**	8.167E-01	8.033E-01	8.068E-01	8.158E-01	8.464E-01
		Std	1.957E-02	3.543E-02	1.876E-02	5.253E-02	**1.153E-02**	2.726E-02	2.801E-02	4.221E-02	3.745E-02	2.268E-02
	10	*Avg*	**8.853E-01**	8.780E-01	8.668E-01	8.447E-01	8.734E-01	8.574E-01	8.344E-01	8.389E-01	8.348E-01	8.719E-01
		Std	**1.280E-02**	1.866E-02	1.709E-02	3.688E-02	1.675E-02	2.352E-02	2.233E-02	3.630E-02	2.894E-02	2.204E-02
	15	*Avg*	**9.391E-01**	9.271E-01	9.076E-01	9.086E-01	9.239E-01	9.016E-01	8.732E-01	8.774E-01	8.766E-01	9.283E-01
		Std	**9.141E-03**	1.440E-02	1.499E-02	3.021E-02	1.227E-02	3.456E-02	2.236E-02	3.899E-02	4.475E-02	1.576E-02
	18	*Avg*	**9.588E-01**	9.517E-01	9.268E-01	9.108E-01	9.332E-01	9.196E-01	9.029E-01	9.116E-01	9.053E-01	9.389E-01
		Std	**4.757E-03**	6.966E-03	1.537E-02	3.865E-02	1.540E-02	1.899E-02	1.910E-02	2.450E-02	1.895E-02	1.317E-02
	20	*Avg*	**9.659E-01**	9.609E-01	9.363E-01	9.236E-01	9.441E-01	9.386E-01	9.035E-01	9.024E-01	9.020E-01	9.480E-01
		Std	6.428E-03	**5.998E-03**	1.564E-02	2.062E-02	1.348E-02	1.690E-02	2.002E-02	3.312E-02	2.035E-02	1.093E-02

Appendix A.7

Comparison of mean values acquired by the Friedman test for PSNR, SSIM and FSIM results.

Image	K	VMCSA	CSA	DE	HHO	PSO	CS	BLPSO	IWOA	IGWO	CGPSO
PSNR	8	**7.79167**	7.10833	5.18333	4.55000	7.27500	4.48333	3.70833	3.76667	3.64167	7.49167
	10	**8.38333**	7.12500	5.50000	4.46667	6.53333	5.05833	3.20000	3.60833	3.70833	7.41667
	15	**8.97500**	7.87500	5.05833	4.68333	6.47500	4.85833	2.65833	3.80833	3.27500	7.33333
	18	**9.20833**	8.62500	5.40833	4.03333	6.37500	4.80833	3.00000	3.38333	2.96667	7.19167
	20	**9.16667**	8.69167	5.56667	4.27500	5.92500	5.01667	3.16667	3.33333	3.14167	6.71667
SSIM	8	**6.56667**	6.36667	4.86667	5.67500	6.13333	5.50000	4.08333	4.51667	4.90000	6.39167
	10	**7.35000**	6.69167	5.08333	5.60000	5.90833	5.41667	3.52500	4.27500	4.44167	6.70833
	15	**8.45833**	7.52500	4.56667	5.31667	6.39167	4.93333	2.72500	4.14167	3.70000	7.24167
	18	**8.95833**	8.30833	4.86667	4.80000	6.17500	4.92500	2.83333	3.78333	3.30833	7.04167
	20	**9.15833**	8.58333	5.35833	4.67500	5.72500	5.04167	2.78333	3.55000	3.30833	6.81667
FSIM	8	**7.45000**	7.03333	4.86667	5.18333	6.91667	4.97500	3.39167	4.15000	3.95833	7.07500
	10	**8.35000**	7.18333	5.09167	4.85000	6.48333	5.26667	3.00833	3.65833	3.84167	7.26667
	15	**9.30833**	7.83333	4.90833	4.87500	6.56667	4.85000	2.45833	3.69167	3.28333	7.22500
	18	**9.54167**	8.59167	5.29167	4.27500	6.35833	4.80833	2.94167	3.28333	2.91667	6.99167
	20	**9.49167**	8.77500	5.56667	4.25833	6.02500	5.01667	2.99167	3.33333	3.15833	6.38333

References

Abd Elaziz, M., Lu, S., & He, S. (2021). A multi-leader whale optimization algorithm for global optimization and image segmentation. *Expert Systems with Applications, 175*.

Abdel-Basset, M., Chang, V., & Mohamed, R. (2020). HSMA_WOA: A hybrid novel Slime mould algorithm with whale optimization algorithm for tackling the image segmentation problem of chest X-ray images. *Applied Soft Computing, 95*, 106642.

Abutaleb, A. S. (1989). Automatic thresholding of gray-level pictures using two-dimensional entropy. *Computer Vision, Graphics, and Image Processing, 47*, 22–32.

Al-Thanoon, N. A., Algamal, Z. Y., & Qasim, O. S. (2021). Feature selection based on a crow search algorithm for big data classification. *Chemometrics and Intelligent Laboratory Systems, 212*, 104288.

Ahmadianfar, I., Heidari, A. A., Gandomi, A. H., Chu, X., & Chen, H. (2021). RUN beyond the metaphor: An efficient optimization algorithm based on Runge Kutta method. *Expert Systems with Applications, 181*, 115079.

Ahmadianfar, I., Heidari, A. A., Noshadian, S., Chen, H., & Gandomi, A. H. (2022). INFO: An efficient optimization algorithm based on weighted mean of vectors. *Expert Systems with Applications*, 116516.

Alcalá-Fdez, J., Sánchez, L., García, S., del Jesus, M. J., Ventura, S., Garrell, J. M., … Herrera, F. (2009). KEEL: A software tool to assess evolutionary algorithms for data mining problems. *Soft Computing, 13*, 307–318.

Amyar, A., Modzelewski, R., Li, H., & Ruan, S. (2020). Multi-task deep learning based CT imaging analysis for COVID-19 pneumonia: Classification and segmentation. *Computers in Biology and Medicine, 126*, 104037.

Aneja, P., Singh, I., Singh, B., Singh Kundi, P., Singh, I., Kathiravan, S., & Mohan Singh, S. (2021). Physicians reactions To Covid-19: The results of a preliminary international internet survey. *Psychiatria Danubina, 33*, 620–625.

Aranguren, I., Valdivia, A., Morales-Castañeda, B., Oliva, D., Abd Elaziz, M., & Perez-Cisneros, M. (2021). Improving the segmentation of magnetic resonance brain images using the LSHADE optimization algorithm. *Biomedical Signal Processing and Control, 64*, 102259.

Askarzadeh, A. (2016). A novel metaheuristic method for solving constrained engineering optimization problems: Crow search algorithm. *Computers & Structures, 169*, 1–12.

Buades, A., Coll, B., & Morel, J. (2005). A non-local algorithm for image denoising. In *2005 IEEE computer society conference on computer vision and pattern recognition (CVPR'05)* (Vol. 2, pp. 60-65 vol. 62).

Bujok, P., & Kolenovsky, P. (2021). Differential evolution with distance-based mutation-selection applied to CEC 2021 single objective numerical optimisation. In *2021 IEEE Congress on Evolutionary Computation (CEC)* (pp. 849–856). IEEE.

Cai, L., Xiong, L., Cao, J., Zhang, H., & Alsaadi, F. E. (2022). State quantized sampled-data control design for complex-valued memristive neural networks. *Journal of the Franklin Institute, 359*, 4019–4053.

Cai, Z., Gu, J., Luo, J., Zhang, Q., Chen, H., Pan, Z., … Li, C. (2019). Evolving an optimal kernel extreme learning machine by using an enhanced grey wolf optimization strategy. *Expert Systems with Applications, 138*, 112814.

Cai, Z., Gu, J., Wen, C., Zhao, D., Huang, C., Huang, H., … Chen, H. (2018). An intelligent Parkinson's disease diagnostic system based on a chaotic bacterial foraging optimization enhanced fuzzy KNN approach. *Computational and Mathematical Methods in Medicine, 2018*, 2396952.

Cao, B., Gu, Y., Lv, Z., Yang, S., Zhao, J., & Li, Y. (2021). RFID reader anticollision based on distributed parallel particle swarm optimization. *IEEE Internet of Things Journal, 8*, 3099–3107.

Cao, B., Zhao, J., Liu, X., Arabas, J., Tanveer, M., Singh, A. K., & Lv, Z. (2022). Multiobjective evolution of the explainable fuzzy rough neural network with gene expression programming. *IEEE Transactions on Fuzzy Systems, 30*(10), 4190–4200.

Cao, L., Yue, Y., Zhang, Y., & Cai, Y. (2021). Improved crow search algorithm optimized extreme learning machine based on classification algorithm and application. *IEEE Access, 9*, 20051–20066.

Cao, X., Sun, X., Xu, Z., Zeng, B., & Guan, X. (2021). Hydrogen-based networked microgrids planning through two-stage stochastic programming with mixed-integer conic recourse. *IEEE Transactions on Automation Science and Engineering*, 1–14.

Cao, X., Wang, J., & Zeng, B. (2022). A study on the strong duality of second-order conic relaxation of AC optimal power flow in radial networks. *IEEE Transactions on Power Systems, 37*, 443–455.

Cao, Z., Wang, Y., Zheng, W., Yin, L., Tang, Y., Miao, W., … Yang, B. (2022). The algorithm of stereo vision and shape from shading based on endoscope imaging. *Biomedical Signal Processing and Control, 76*, 103658.

Chaudhuri, A., & Sahu, T. P. (2021). Feature selection using Binary Crow Search Algorithm with time varying flight length. *Expert Systems with Applications, 168*, 114288.

Chen, C., Wang, X., Yu, H., Zhao, N., Wang, M., & Chen, H. (2020). An enhanced comprehensive learning particle swarm optimizer with the elite-based dominance scheme. *Complexity, 2020*, 4968063.

Chen, L., Zheng, Z., Liu, H. L., & Xie, S. (2014). An evolutionary algorithm based on Covariance Matrix Leaning and Searching Preference for solving CEC 2014 benchmark problems. In *Proceedings of the 2014 IEEE congress on evolutionary computation* (pp. 2672–2677).

Chen, X., Tianfield, H., Mei, C., Du, W., & Liu, G. (2017). Biogeography-based learning particle swarm optimization. *Soft Computing, 21*, 7519–7541.

Chen, X., Yao, L., Zhou, T., Dong, J., & Zhang, Y. (2021). Momentum contrastive learning for few-shot COVID-19 diagnosis from chest CT images. *Pattern Recognition, 113*, 107826.

Chen, Y., Yang, X.-H., Wei, Z., Heidari, A. A., Zheng, N., Li, Z., … Guan, Q. (2022). Generative Adversarial Networks in Medical Image augmentation: A review. *Computers in Biology and Medicine, 144*, 105382.

Chon, J., & Kim, H. (2006). Robust fault matched optical flow detection using 2D histogram. In M. Gavrilova, O. Gervasi, V. Kumar, C. J. K. Tan, D. Taniar, A. Lagana, Y. Mun & H. Choo (Eds.), *Computational science and its applications - Iccsa 2006, Pt 3* (Vol. 3982, pp. 1172-1179).

Cohen, J. P., Morrison, P., Dao, L., Roth, K., Duong, T. Q., & Ghassemi, M. (2020). Covid-19 image data collection: Prospective predictions are the future. *[Online]. Available.* https://github.com/ieee8023/covid-chestxray-dataset.

Deng, W., Zhang, X., Zhou, Y., Liu, Y., Zhou, X., Chen, H., & Zhao, H. (2022). An enhanced fast non-dominated solution sorting genetic algorithm for multi-objective problems. *Information Sciences, 585*, 441–453.

Di Buo, A., Moretti, P., Menculini, G., Minuti, A., Valentini, E., Cerasoli, I., … Gerli, S. (2021). Antepartum Distress during COVID-19 Pandemic: An Observational Study. *Psychiatria Danubina, 33*, 137–141.

Di, D., Shi, F., Yan, F., Xia, L., Mo, Z., Ding, Z., … Shen, D. (2021). Hypergraph learning for identification of COVID-19 with CT imaging. *Medical Image Analysis, 68*, Article 101910.

Diaz, P., Perez-Cisneros, M., Cuevas, E., Avalos, O., Galvez, J., Hinojosa, S., & Zaldivar, D. (2018). An improved crow search algorithm applied to energy problems. *Energies, 11*(3), 571.

Dong, B., Jin, R., & Weng, G. (2019). Active contour model based on local bias field estimation for image segmentation. *Signal Processing-Image Communication, 78*, 187–199.

Dong, R., Chen, H., Heidari, A. A., Turabieh, H., Mafarja, M., & Wang, S. (2021). Boosted kernel search: Framework, analysis and case studies on the economic emission dispatch problem. *Knowledge-Based Systems, 233*, 107529.

Elhosseini, M. A., Haikal, A. Y., Badawy, M., & Khashan, N. (2019). Biped robot stability based on an A-C parametric Whale Optimization Algorithm. *Journal of Computational Science, 31*, 17–32.

Eliguzel, I. M., & Ozceylan, E. (2021). Application of an improved discrete crow search algorithm with local search and elitism on a humanitarian relief case. *Artificial Intelligence Review, 54*(6), 4591–4617.

Fan, Q., Zhang, Z., & Huang, X. (2022). Parameter conjugate gradient with secant equation based Elman neural network and its convergence analysis. *Advanced Theory and Simulations*, 2200047.
Farh, H. M. H., Eltamaly, A. M., Al-Shaalan, A. M., & Al-Shamma'a, A. A. (2021). A novel sizing inherits allocation strategy of renewable distributed generations using crow search combined with particle swarm optimization algorithm. *Iet Renewable Power Generation, 15*, 1436–1450.
Gandomi, A. H., Yang, X.-S., & Alavi, A. H. (2013). Cuckoo search algorithm: A metaheuristic approach to solve structural optimization problems. *Engineering with Computers, 29*, 17–35.
García, S., Fernández, A., Luengo, J., & Herrera, F. (2010). Advanced nonparametric tests for multiple comparisons in the design of experiments in computational intelligence and data mining: Experimental analysis of power. *Information Sciences, 180*, 2044–2064.
Gholami, J., Mardukhi, F., & Zawbaa, H. M. (2021). An improved crow search algorithm for solving numerical optimization functions. *Soft Computing, 25*(14), 9441–9454.
Guan, Q., Chen, Y., Wei, Z., Heidari, A. A., Hu, H., Yang, X.-H., … Chen, F. (2022). Medical image augmentation for lesion detection using a texture-constrained multichannel progressive GAN. *Computers in Biology and Medicine, 145*, 105444.
Guan, R., Zhang, H., Liang, Y., Giunchiglia, F., Huang, L., & Feng, X. (2020). Deep feature-based text clustering and its explanation. *IEEE Transactions on Knowledge and Data Engineering*, 1-1.
Gupta, S., & Deep, K. (2019). A hybrid self-adaptive sine cosine algorithm with opposition based learning. *Expert Systems with Applications, 119*, 210–230.
Hansen, P., Mladenovic, N., & Perez, J. A. M. (2008). Variable neighborhood search. *European Journal of Operational Research, 191*, 593–595.
He, Z., Yen, G. G., & Ding, J. (2020). Knee-based decision making and visualization in many-objective optimization. *IEEE Transactions on Evolutionary Computation, 25*, 292–306.
He, Z., Yen, G. G., & Lv, J. (2019). Evolutionary multiobjective optimization with robustness enhancement. *IEEE Transactions on Evolutionary Computation, 24*, 494–507.
He, Z., Yen, G. G., & Yi, Z. (2018). Robust multiobjective optimization via evolutionary algorithms. *IEEE Transactions on Evolutionary Computation, 23*, 316–330.
Heidari, A. A., Aljarah, I., Faris, H., Chen, H., Luo, J., & Mirjalili, S. (2019). An enhanced associative learning-based exploratory whale optimizer for global optimization. *Neural Computing and Applications, 9*, 5185–5211.
Heidari, A. A., Mirjalili, S., Faris, H., Aljarah, I., Mafarja, M., & Chen, H. (2019). Harris hawks optimization: Algorithm and applications. *Future Generation Computer Systems, 97*, 849–872.
Houssein, E. H., Helmy, B.-E.-D., Oliva, D., Elngar, A. A., & Shaban, H. (2021). A novel Black Widow Optimization algorithm for multilevel thresholding image segmentation. *Expert Systems with Applications, 167*.
Hu, J., Chen, H., Heidari, A. A., Wang, M., Zhang, X., Chen, Y., & Pan, Z. (2021). Orthogonal learning covariance matrix for defects of grey wolf optimizer: Insights, balance, diversity, and feature selection. *Knowledge-Based Systems, 213*, Article 106684.
Hu, J., Gui, W., Heidari, A. A., Cai, Z., Liang, G., Chen, H., & Pan, Z. (2022). Dispersed foraging slime mould algorithm: Continuous and binary variants for global optimization and wrapper-based feature selection. *Knowledge-Based Systems, 237*, Article 107761.
Hua, Y., Liu, Q., Hao, K., & Jin, Y. (2021). A survey of evolutionary algorithms for multi-objective optimization problems with irregular Pareto fronts. *IEEE/CAA Journal of Automatica Sinica, 8*, 303–318.
Huang, L., Yang, Y., Chen, H., Zhang, Y., Wang, Z., & He, L. (2022). Context-aware road travel time estimation by coupled tensor decomposition based on trajectory data. *Knowledge-Based Systems, 245*, Article 108596.
Hussien, A. G., Heidari, A. A., Ye, X., Liang, G., Chen, H., & Pan, Z. (2022). Boosting whale optimization with evolution strategy and Gaussian random walks: An image segmentation method. *Engineering with Computers*. https://doi.org/10.1007/s00366-021-01542-0
Huynh-Thu, Q., & Ghanbari, M. (2008). Scope of validity of PSNR in image/video quality assessment. *Electronics Letters, 44*, 800–U835.
Jain, M., Rani, A., & Singh, V. (2017). An improved Crow Search Algorithm for high-dimensional problems. *Journal of Intelligent & Fuzzy Systems, 33*, 3597–3614.
Jalušić Glunčić, T., Muršić, D., Basara, L., Vranić, L., Moćan, A., Janković Makek, M., & Samaržija, M. (2021). Overview of symptoms of ongoing symptomatic and post-COVID-19 patients who were reffered to pulmonary rehabilitation-first single-centre experience in Croatia. *Psychiatria Danubina, 33*, 565–571.
Kalyani, R., Sathya, P. D., & Sakthivel, V. P. (2021). Multilevel thresholding for image segmentation with exchange market algorithm. *Multimedia Tools and Applications, 80* (18), 27553–27591.
Ke, Y., Xie, J., & Pouramini, S. (2021). Utilization of an improved crow search algorithm to solve building energy optimization problems: Cases of Australia. *Journal of Building Engineering, 38*.
Kennedy, J., & Eberhart, R. (1995). Particle swarm optimization. In *IEEE International conference on neural networks - conference proceedings* (Vol. 4, pp. 1942-1948).
Khairuzzaman, A. K. M., & Chaudhury, S. (2020). Modified moth-flame optimization algorithm-based multilevel minimum cross entropy thresholding for image segmentation. *International Journal of Swarm Intelligence Research, 11*, 123–139.
Khalilpourazari, S., & Pasandideh, S. H. R. (2020). Sine-cosine crow search algorithm: Theory and applications. *Neural Computing & Applications, 32*, 7725–7742.
Kim, S. W., Choi, B. D., Park, W. J., & Ko, S. J. (2016). 2D histogram equalisation based on the human visual system. *Electronics Letters, 52*, 443–444.
Kumar, S., Vig, G., Varshney, S., & Bansal, P. (2020). Brain tumor detection based on multilevel 2D histogram image segmentation using DEWO optimization algorithm. *International Journal of E-Health and Medical Communications, 11*, 71–85.
Li, D., Zhang, S., & Ma, X. (2021). Dynamic module detection in temporal attributed networks of cancers. *IEEE/ACM Transactions on Computational Biology and Bioinformatics*. https://doi.org/10.1109/TCBB.2021.3069441
Li, J.-Y., Zhan, Z.-H., Wang, C., Jin, H., & Zhang, J. (2020). Boosting data-driven evolutionary algorithm with localized data generation. *IEEE Transactions on Evolutionary Computation, 24*, 923–937.
Li, J., Chen, C., Chen, H., & Tong, C. (2017). Towards context-aware social recommendation via individual trust. *Knowledge-Based Systems, 127*, 58–66.
Li, J., & Lin, J. (2020). A probability distribution detection based hybrid ensemble QoS prediction approach. *Information Sciences, 519*, 289–305.
Li, J., Zheng, X.-L., Chen, S.-T., Song, W.-W., & Chen, D.-R. (2014). An efficient and reliable approach for quality-of-service-aware service composition. *Information Sciences, 269*, 238–254.
Li, L., Gao, Z., Wang, Y.-T., Zhang, M.-W., Ni, J.-C., Zheng, C.-H., & Su, Y. (2021). SCMFMDA: Predicting microRNA-disease associations based on similarity constrained matrix factorization. *Plos Computational Biology, 17*, e1009165.
Li, Q., Chen, H., Huang, H., Zhao, X., Cai, Z., Tong, C., … Tian, X. (2017). An enhanced grey wolf optimization based feature selection wrapped kernel extreme learning machine for medical diagnosis. *Computational and Mathematical Methods in Medicine, 2017*, 9512741.
Li, S., Chen, H., Wang, M., Heidari, A. A., & Mirjalili, S. (2020). Slime mould algorithm: A new method for stochastic optimization. *Future Generation Computer Systems-the International Journal of Escience, 111*, 300–323.
Chen, H., Yang, B., Wang, S., Wang, G., & zhong Li, H., and Liu, W.. (2014). Towards an optimal support vector machine classifier using a parallel particle swarm optimization strategy. *Applied Mathematics and Computation, 239*, 180–197.
Liang, J. J., Qu, B. Y., & Suganthan, P. N. (2013). *Problem definitions and evaluation criteria for the CEC 2014 special session and competition on single objective real-parameter numerical optimization, 635* p. 490). Singapore: Computational Intelligence Laboratory, Zhengzhou University, Zhengzhou China and Technical Report, Nanyang Technological University.
Liu, K., Ke, F., Huang, X., Yu, R., Lin, F., Wu, Y., & Ng, D. W. K. (2021). DeepBAN: A temporal convolution-based communication framework for dynamic WBANs. *IEEE Transactions on Communications, 69*, 6675–6690.
Liu, S., Yang, B., Wang, Y., Tian, J., Yin, L., & Zheng, W. (2022). 2D/3D multimode medical image registration based on normalized cross-correlation. *Applied Sciences, 12*, 2828.
Lu, C., Liu, Q., Zhang, B., & Yin, L. (2022). A Pareto-based hybrid iterated greedy algorithm for energy-efficient scheduling of distributed hybrid flowshop. *Expert Systems with Applications*, 117555.
Luo, J., Yang, Y., & Shi, B. (2019). Multi-threshold image segmentation of 2D Otsu based on improved adaptive differential evolution algorithm. *Journal of Electronics & Information Technology, 41*, 2017–2024.
Lv, Z., Yu, Z., Xie, S., & Alamri, A. (2022). Deep learning-based smart predictive evaluation for interactive multimedia-enabled smart healthcare. *ACM Transactions on Multimedia Computing, Communications, and Applications (TOMM), 18*, 1–20.
Ma, X., Sun, P. G., & Gong, M. (2020). An integrative framework of heterogeneous genomic data for cancer dynamic modules based on matrix decomposition. *IEEE/ACM Transactions on Computational Biology and Bioinformatics*. https://doi.org/10.1109/TCBB.2020.3004808
Merzban, M. H., & Elbayoumi, M. (2019). Efficient solution of Otsu multilevel image thresholding: A comparative study. *Expert Systems with Applications, 116*, 299–309.
Michetti, J., Georgelin-Gurgel, M., Mallet, J. P., Diemer, F., & Boulanouar, K. (2015). Influence of CBCT parameters on the output of an automatic edge-detection-based endodontic segmentation. *Dentomaxillofacial Radiology, 44*, 20140413.
Mirjalili, S., Dong, J. S., & Lewis, A. (2019). *Nature-inspired optimizers: theories, literature reviews and applications* (Vol. 811). Springer.
Mittal, H., & Saraswat, M. (2018). An optimum multi-level image thresholding segmentation using non-local means 2D histogram and exponential Kbest gravitational search algorithm. *Engineering Applications of Artificial Intelligence, 71*, 226–235.
Mukhtar, S., & Rana, W. (2021). Biopsychosocial-spiritual model of COVID-19 for healthcare practitioners amidst and post-COVID-19. *Psychiatria Danubina, 33*, 595–599.
Necira, A., Naimi, D., Salhi, A., Salhi, S., & Menani, S. (2021). Dynamic crow search algorithm based on adaptive parameters for large-scale global optimization. *Evolutionary Intelligence, 15*(3), 2153–2169.
Nenavath, H., & Jatoth, R. K. (2018). Hybridizing sine cosine algorithm with differential evolution for global optimization and object tracking. *Applied Soft Computing Journal, 62*, 1019–1043.
Nobre, R. H., Rodrigues, F. A. A., Marques, R. C. P., Nobre, J. S., Neto, J., & Medeiros, F. N. S. (2016). SAR image segmentation with Rnyis entropy. *IEEE Signal Processing Letters, 23*, 1551–1555.
Ouadfel, S., & Abd Elaziz, M. (2020). Enhanced crow search algorithm for feature selection. *Expert Systems with Applications, 159*, Article 113572.
Qiu, S., Hao, Z., Wang, Z., Liu, L., Liu, J., Zhao, H., & Fortino, G. (2021). Sensor combination selection strategy for Kayak cycle phase segmentation based on body sensor networks. *IEEE Internet of Things Journal, 9*, 4190–4201. https://doi.org/10.1109/JIOT.2021.3102856
Qiu, S., Zhao, H., Jiang, N., Wu, D., Song, G., Zhao, H., & Wang, Z. (2021). Sensor network oriented human motion capture via wearable intelligent system. *International Journal of Intelligent Systems, 37*(2), 1646–1673. https://doi.org/10.1002/int.22689

Qu, C., & Fu, Y. (2019). Crow search algorithm based on neighborhood search of non-inferior solution set. *IEEE Access, 7*, 52871–52895.
Rahaman, J., & Sing, M. (2021). An efficient multilevel thresholding based satellite image segmentation approach using a new adaptive cuckoo search algorithm. *Expert Systems with Applications, 174*, Article 114633.
Renugambal, A., & Selva Bhuvaneswari, K. (2021). Kapur's entropy based hybridised WCMFO algorithm for brain MR image segmentation. *IETE Journal of Research*. https://doi.org/10.1080/03772063.2021.1906765
Rizk-Allah, R. M., Hassanien, A. E., & Bhattacharyya, S. (2018). Chaotic crow search algorithm for fractional optimization problems. *Applied Soft Computing, 71*, 1161–1175.
Shubham, S., & Bhandari, A. K. (2019). A generalized Masi entropy based efficient multilevel thresholding method for color image segmentation. *Multimedia Tools and Applications, 78*, 17197–17238.
Singla, A., Patra, S. J. S., Image, & Processing, V. (2017). A fast automatic optimal threshold selection technique for image segmentation. *11*, 243-250.
Storn, R., & Price, K. (1997). Differential evolution - A simple and efficient heuristic for global optimization over continuous spaces. *Journal of Global Optimization, 11*, 341–359.
Su, Y., Li, S., Zheng, C., & Zhang, X. (2019). A heuristic algorithm for identifying molecular signatures in cancer. *IEEE Transactions on Nanobioscience, 19*, 132–141.
Tu, J., Chen, H., Wang, M., & Gandomi, A. H. (2021). The colony predation algorithm. *Journal of Bionic Engineering, 18*, 674–710.
Tubishat, M., Abushariah, M. A. M., Idris, N., & Aljarah, I. (2019). Improved whale optimization algorithm for feature selection in Arabic sentiment analysis. *Applied Intelligence, 49*, 1688–1707.
Upadhyay, P., & Chhabra, J. K. (2020). Kapur's entropy based optimal multilevel image segmentation using Crow Search Algorithm. *Applied soft computing, 97*.
Wang, D., Liang, Y., Xu, D., Feng, X., & Guan, R. (2018). A content-based recommender system for computer science publications. *Knowledge-Based Systems, 157*, 1–9.
Wang, G., Gui, W., Liang, G., Zhao, X., Wang, M., Mafarja, M., … Ma, X. (2021). Spiral motion enhanced elite whale optimizer for global tasks. *Complexity, 2021*, 8130378.
Wang, W., Chen, Z., & Yuan, X. (2022). Simple low-light image enhancement based on Weber-Fechner law in logarithmic space. *Signal Processing: Image Communication*, 116742.
Wang, Z., Bovik, A. C., Sheikh, H. R., & Simoncelli, E. P. (2004). Image quality assessment: From error visibility to structural similarity. *IEEE Transactions on Image Processing, 13*, 600–612.
Wolpert, D. H., & Macready, W. G. (1997). No free lunch theorems for optimization. *IEEE Transactions on Evolutionary Computation, 1*, 67–82.
Wu, G., Mallipeddi, R., Suganthan, P. N., National University of Defense Technology, Changsha, Hunan, PR China and Kyungpook National University, Daegu, *South Korea and Nanyang Technological University, Singapore, Technical Report*. (2017). Problem definitions and evaluation criteria for the CEC 2017 competition on constrained real-parameter optimization.
Wu, Q.-W., Cao, R.-F., Xia, J., Ni, J.-C., Zheng, C.-H., & Su, Y. (2021). Extra trees method for predicting LncRNA-disease association based on multi-layer graph embedding aggregation. *IEEE/ACM transactions on computational biology and bioinformatics*. https://doi.org/10.1109/TCBB.2021.3113122
Wu, S.-H., Zhan, Z.-H., & Zhang, J. (2021). SAFE: Scale-adaptive fitness evaluation method for expensive optimization problems. *IEEE Transactions on Evolutionary Computation, 25*, 478–491.
Wu, X., Zheng, W., Chen, X., Zhao, Y., Yu, T., & Mu, D. (2021). Improving high-impact bug report prediction with combination of interactive machine learning and active learning. *Information and Software Technology, 133*, Article 106530.
Wu, Z., Li, G., Shen, S., Cui, Z., Lian, X., & Xu, G. (2021). Constructing dummy query sequences to protect location privacy and query privacy in location-based services. *World Wide Web, 24*, 25–49.
Wu, Z., Li, R., Xie, J., Zhou, Z., Guo, J., & Xu, X. (2020). A user sensitive subject protection approach for book search service. *Journal of the Association for Information Science and Technology, 71*, 183–195.
Wu, Z., Shen, S., Lian, X., Su, X., & Chen, E. (2020). A dummy-based user privacy protection approach for text information retrieval. *Knowledge-Based Systems, 195*, 105679.
Wu, Z., Shen, S., Zhou, H., Li, H., Lu, C., & Zou, D. (2021). An effective approach for the protection of user commodity viewing privacy in e-commerce website. *Knowledge-Based Systems, 220*, 106952.
Wu, Z., Wang, R., Li, Q., Lian, X., & Xu, G. (2020). A location privacy-preserving system based on query range cover-up for location-based services. *IEEE Transactions on Vehicular Technology, 69*.
Xia, X., Liu, Q., & Huang, M. L. (2021). The use of artificial intelligence based magnifying image segmentation algorithm combined with endoscopy in early diagnosis and nursing of esophageal cancer patients. *Journal of Medical Imaging and Health Informatics, 11*, 1306–1311.
Xu, Q., Zeng, Y., Tang, W., Peng, W., Xia, T., Li, Z., … Guo, J. (2020). Multi-task joint learning model for segmenting and classifying tongue images using a deep neural network. *IEEE Journal of Biomedical and Health Informatics, 24*, 2481–2489.
Xu, Y., Chen, H., Heidari, A. A., Luo, J., Zhang, Q., Zhao, X., & Li, C. (2019). An efficient chaotic mutative moth-flame-inspired optimizer for global optimization tasks. *Expert Systems with Applications, 129*, 135–155.
Yan, Z., Zhang, J., & Tang, J. (2020). Modified water wave optimization algorithm for underwater multilevel thresholding image segmentation. *Multimedia Tools and Applications, 79*, 32415–32448.
Yang, Y., Chen, H., Heidari, A. A., & Gandomi, A. H. (2021). Hunger games search: Visions, conception, implementation, deep analysis, perspectives, and towards performance shifts. *Expert Systems with Applications, 177*, 114864.
Ye, X., Liu, W., Li, H., Wang, M., Chi, C., Liang, G., … Huang, H. (2021). Modified whale optimization algorithm for solar cell and PV module parameter identification. *Complexity, 2021*, 8878686.
Yimit, A., & Hagihara, Y. (2018). 2D direction histogram-based Renyi entropic multilevel thresholding. *Journal of Advanced Computational Intelligence and Intelligent Informatics, 22*, 369–379.
Yin, J., Sun, W., Li, F., Hong, J., Li, X., Zhou, Y., … Zhu, F. (2020). VARIDT 1.0: Variability of drug transporter database. *Nucleic Acids Research, 48*, D1042–D1050.
Yin, S. B., Qian, Y. M., & Gong, M. L. (2017). Unsupervised hierarchical image segmentation through fuzzy entropy maximization. *Pattern Recognition, 68*, 245–259.
Yu, H., Cheng, X., Chen, C., Heidari, A. A., Liu, J., Cai, Z., & Chen, H. (2022). Apple leaf disease recognition method with improved residual network. *Multimedia Tools and Applications*.
Yu, H., Song, J., Chen, C., Heidari, A. A., Liu, J., Chen, H., … Mafarja, M. (2022). Image segmentation of Leaf Spot Diseases on Maize using multi-stage Cauchy-enabled grey wolf algorithm. *Engineering Applications of Artificial Intelligence, 109*, 104653.
Yu, H., Yuan, K., Li, W., Zhao, N., Chen, W., Huang, C., … Wang, M. (2021). Improved butterfly optimizer-configured extreme learning machine for fault diagnosis. *Complexity, 2021*, 6315010.
Yu, H. Y., Zhi, X. B., & Fan, J. L. (2015). Image segmentation based on weak fuzzy partition entropy. *Neurocomputing, 168*, 994–1010.
Zhang, D., Liu, Y., Yang, Y., Xu, M., Yan, Y., & Qin, Q. (2016). A region-based segmentation method for ultrasound images in HIFU therapy. *Medical Physics, 43*, 2975–2989.
Zhang, J., Hong, L., & Liu, Q. (2020). An improved whale optimization algorithm for the traveling salesman problem. *Symmetry, 13*(1), 48.
Zhang, L., Zhang, L., Mou, X., & Zhang, D. (2011). FSIM: A feature similarity index for image quality assessment. *IEEE Transactions on Image Processing, 20*, 2378–2386.
Zhang, M., Chen, Y., & Lin, J. (2021). A privacy-preserving optimization of neighborhood-based recommendation for medical-aided diagnosis and treatment. *IEEE Internet of Things Journal, 8*, 10830–10842.
Zhang, M., Chen, Y., & Susilo, W. (2020). PPO-CPQ: A privacy-preserving optimization of clinical pathway query for e-healthcare systems. *IEEE Internet of Things Journal, 7*, 10660–10672.
Zhang, X., Fan, C., Xiao, Z., Zhao, L., Chen, H., & Chang, X. (2022). Random reconstructed unpaired image-to-image translation. *IEEE Transactions on Industrial Informatics*. https://doi.org/10.1109/TII.2022.3160705
Zhang, X., Wang, J., Wang, T., & Jiang, R. (2021). Hierarchical feature fusion with mixed convolution attention for single image dehazing. *IEEE Transactions on Circuits and Systems for Video Technology*. https://doi.org/10.1109/TCSVT.2021.3067062
Zhang, Z., Wang, L., Zheng, W., Yin, L., Hu, R., & Yang, B. (2022). Endoscope image mosaic based on pyramid ORB. *Biomedical Signal Processing and Control, 71*, 103261.
Zhao, D., Liu, L., Yu, F., Heidari, A. A., Wang, M., Liang, G., … Chen, H. (2020). Chaotic random spare ant colony optimization for multi-threshold image segmentation of 2D Kapur entropy. *Knowledge-Based Systems*, 106510. https://doi.org/10.1016/j.knosys.102020.106510
Zhao, D., Liu, L., Yu, F., Heidari, A. A., Wang, M., Oliva, D., … Chen, H. (2020). Ant colony optimization with horizontal and vertical crossover search: Fundamental visions for multi-threshold image segmentation. *Expert Systems with Applications*, 114122.
Zhao, F., Di, S., Cao, J., & Tang, J. (2021). A novel cooperative multi-stage hyper-heuristic for combination optimization problems. *Complex System Modeling and Simulation, 1*, 91–108.
Zhao, S., Wang, P., Heidari, A. A., Chen, H., Turabieh, H., Mafarja, M., & Li, C. (2021). Multilevel threshold image segmentation with diffusion association slime mould algorithm and Renyi's entropy for chronic obstructive pulmonary disease. *Computers in Biology and Medicine, 134*, 104427.
Zhou, L., Fan, Q., Huang, X., & Liu, Y. (2022). Weak and strong convergence analysis of Elman neural networks via weight decay regularization. *Optimization*, 1–23.
Zhou, W., Wang, H., & Wan, Z. (2022). Ore image classification based on improved CNN. *Computers and Electrical Engineering, 99*, 107819.
Zhou, Y., Yang, X., Ling, Y., & Zhang, J. (2018). Meta-heuristic moth swarm algorithm for multilevel thresholding image segmentation. *Multimedia Tools and Applications, 77*, 23699–23727.
Zhu, B., Zhong, Q., Chen, Y., Liao, S., Li, Z., Shi, K., & Sotelo, M. A. (2022). A Novel reconstruction method for temperature distribution measurement based on ultrasonic tomography. *IEEE Transactions on Ultrasonics, Ferroelectrics, and Frequency Control*.
Zhu, F., Shi, Z., Qin, C., Tao, L., Liu, X., Xu, F., … Chen, Y. (2012). Therapeutic target database update 2012: A resource for facilitating target-oriented drug discovery. *Nucleic Acids Research, 40*, D1128–D1136.